© 2018. Published by The Company of Biologists Ltd | Development (2018) 145, dev151571. doi:10.1242/dev.151571

RESEARCH ARTICLE

The phosphoinositide phosphatase Sac1 regulates cell shape and microtubule stability in the developing *Drosophila* eye

Lauren M. Del Bel[1,2], Nigel Griffiths[1,2], Ronit Wilk[1], Ho-Chun Wei[1,3], Anastasia Blagoveshchenskaya[4], Jason Burgess[1,2], Gordon Polevoy[1], James V. Price[3,*], Peter Mayinger[4] and Julie A. Brill[1,2,‡]

ABSTRACT

Epithelial patterning in the developing *Drosophila melanogaster* eye requires the Neph1 homolog Roughest (Rst), an immunoglobulin family cell surface adhesion molecule expressed in interommatidial cells (IOCs). Here, using a novel temperature-sensitive (ts) allele, we show that the phosphoinositide phosphatase Sac1 is also required for IOC patterning. *Sac1^{ts}* mutants have rough eyes and retinal patterning defects that resemble *rst* mutants. *Sac1^{ts}* retinas exhibit elevated levels of phosphatidylinositol 4-phosphate (PI4P), consistent with the role of Sac1 as a PI4P phosphatase. Indeed, genetic rescue and interaction experiments reveal that restriction of PI4P levels by Sac1 is crucial for normal eye development. Rst is delivered to the cell surface in *Sac1^{ts}* mutants. However, *Sac1^{ts}* mutant IOCs exhibit severe defects in microtubule organization, associated with accumulation of Rst and the exocyst subunit Sec8 in enlarged intracellular vesicles upon cold fixation *ex vivo*. Together, our data reveal a novel requirement for Sac1 in promoting microtubule stability and suggest that Rst trafficking occurs in a microtubule- and exocyst-dependent manner.

KEY WORDS: Phosphatidylinositol 4-phosphate, PtdIns(4)P, Exocyst, IRM protein, Sac1, PI4KII, *Drosophila*

INTRODUCTION

Undifferentiated epithelial cells are patterned and specified during development to yield highly ordered tissues composed of multiple cell types. Patterning and differentiation within an epithelium are driven in part by cell surface adhesion molecules that promote intercellular interactions. Defects in cell-cell adhesion lead to developmental abnormalities and contribute to disease progression. For example, the mammalian Irre cell recognition module (IRM) adhesion proteins NEPH1 (KIRREL) and nephrin (NPHS1) are required in the kidney for development and maintenance of the filtration barrier or slit diaphragm (Donoviel et al., 2001; Kestilä et al., 1998; Ruotsalainen et al., 1999). Despite their importance in animal development and physiology, little is known about how trafficking and delivery of cell surface adhesion molecules such as IRM proteins is achieved.

The adult *Drosophila* eye contains ∼750 individual units called ommatidia. Prior to pupariation, each ommatidium consists of eight photoreceptor (PR) cells and four cone cells, surrounded by undifferentiated interommatidial cells (IOCs) (Bao and Cagan, 2005; Cagan and Ready, 1989a,b). During the first half of pupal eye development, 0-42 h after puparium formation (APF), IOCs undergo dynamic morphogenetic changes to give rise to two primary pigment cells (1°pc), six secondary pigment cells (2°pc), three tertiary pigment cells (3°pc) and three bristles, arranged in a honeycomb lattice. These cells support and optically isolate individual ommatidia.

Specification and organization of *Drosophila* retinal cells requires IRM protein function (Araujo et al., 2003; Bao and Cagan, 2005; Bao et al., 2010; Reiter et al., 1996). 1°pc express the nephrin homologs Hibris (Hbs) and Sticks and stones (Sns), whereas IOCs express the NEPH1 homologs Roughest (Rst) and Kin of Irre (Kirre, also called Dumbfounded) (Bao and Cagan, 2005; Bao et al., 2010). Between 24 and 30 h APF, all four proteins localize to the plasma membrane (PM) of these cells at the 1°pc:IOC border, and heterophilic binding of Rst and Kirre with Hbs and Sns is needed for specification and morphogenesis of 2°pc and 3°pc (2°/3°pc) (Bao and Cagan, 2005; Bao et al., 2010; Reiter et al., 1996). Mutations that affect cell surface accumulation of Rst result in rough eyes and reduced levels of pigmentation as a result of defects in 2°/3°pc differentiation (Araujo et al., 2003; Reiter et al., 1996; Wolff and Ready, 1991).

Phosphoinositides, or phosphatidylinositol (PI) phosphates (PIPs), regulate essential cellular processes such as membrane trafficking and actin cytoskeletal organization. In the canonical PIP pathway, PI is phosphorylated by PI 4-kinases (PI4Ks) to generate PI 4-phosphate (PI4P) (Fig. 1A), which is a precursor for other PIPs, including PI 4,5-bisphosphate [PI(4,5)P_2], and serves as a potent signaling molecule, for example by recruiting effectors to the Golgi body to promote membrane trafficking (De Matteis et al., 2013; Delage et al., 2013; Santiago-Tirado and Bretscher, 2011; Tan and Brill, 2014). Downregulation of PI4P in specific membrane compartments also drives cellular events. For example, in budding yeast (*Saccharomyces cerevisiae*), PI4P dephosphorylation is required for targeted delivery of cargo to the PM by the exocyst complex (Ling et al., 2014; Mizuno-Yamasaki et al., 2010). *Drosophila* has three PI4Ks, including a single type II enzyme (PI4KII) that generates PI4P at the *trans*-Golgi network (TGN) and on endosomes (Burgess et al., 2012). PI4P levels are kept in check by the phosphoinositide phosphatase Sac1 (Fig. 1A), a conserved transmembrane protein present in endoplasmic reticulum and Golgi membranes (Forrest et al., 2013; Foti et al., 2001; Guo et al., 1999; Nemoto et al., 2000; Rivas et al., 1999; Whitters et al., 1993).

We previously showed that Sac1 is required for normal eye development in *Drosophila* (Wei et al., 2003b). Sac1 is essential for

[1]Cell Biology Program, The Hospital for Sick Children, PGCRL Building, 686 Bay Street, Toronto, Ontario, M5G 0A4, Canada. [2]Department of Molecular Genetics, University of Toronto, 1 King's College Circle, Toronto, Ontario, M5S 1A8, Canada. [3]Department of Molecular Biology and Biochemistry, Simon Fraser University, South Sciences Building Room 8166, 8888 University Drive, Burnaby, British Columbia, V5A 1S6, Canada. [4]Division of Nephrology & Hypertension, Oregon Health & Science University, 3181 S.W. Sam Jackson Park Rd., Portland, Oregon 97239-3098, USA.
*Present address: Department of Biology, Utah Valley University, 800 West University Parkway, Orem, Utah 84058, USA.

‡Author for correspondence (julie.brill@sickkids.ca)

L.M.D., 0000-0001-7122-0551; R.W., 0000-0002-0982-313X; H.-C.W., 0000-0002-6124-0273; A.B., 0000-0002-0597-7406; J.B., 0000-0003-2909-3506; G.P., 0000-0001-7956-6303; J.V.P., 0000-0001-9068-7317; P.M., 0000-0003-1318-3339; J.A.B., 0000-0002-5925-9901

Received 9 March 2017; Accepted 30 April 2018

Development (2018) 145, dev151571. doi:10.1242/dev.151571

viability in *Drosophila* (Wei et al., 2003a,b). Flies transheterozygous for a hypomorphic allele and a null allele exhibit rough eyes with necrotic patches and drown in the food soon after eclosing (Wei et al., 2003b). Here, using the hypomorphic allele, which we show is temperature sensitive (ts), we demonstrate that Sac1 plays a crucial role in patterning the retinal epithelium. IOCs of $Sac1^{ts}$ flies cultured at 25°C exhibit a dramatic increase in PI4P levels and decreased levels of PM PI(4,5)P_2. Although Rst is present at the cell surface of these IOCs, fixation on ice *ex vivo* results in re-distribution of Rst to enlarged structures containing the exocyst complex subunit Sec8, suggesting a microtubule defect. Indeed, $Sac1^{ts}$ IOCs contain sparse, disorganized microtubules (MTs) that disappear when fixed on ice. Our results thus identify a novel link between Sac1, PIP levels and microtubule stability in the developing *Drosophila* eye. Because Sac1 is conserved, our findings suggest a possible role for MT regulation by Sac1 in human development and disease.

RESULTS

Sac1 is required for normal eye development

We discovered that a hypomorphic allele of *Sac1*, isolated in a screen to identify lethal mutations in the 61D-61F region of *Drosophila* chromosome III (Wei et al., 2003b), was temperature sensitive (ts) ($Sac1^{ts}$; previously called $l(3)2107^{L4H}$). The $Sac1^{ts}$ mutation causes an amino acid substitution (G382R) within the Sac phosphatase domain, six amino acids upstream of the catalytic motif (Fig. 1B). To determine whether the G382R (TS) mutation affects Sac1 protein stability, Flag-tagged wild-type (WT), phosphatase-reduced (PR; C391S) and TS versions of *Drosophila* Sac1 were expressed in HeLa cells (Fig. 1C). All three constructs yielded similar amounts of Sac1 protein when cells were grown at 25°C; however, when grown at 37°C, cells expressing the TS construct had nearly undetectable levels of Sac1. To examine the catalytic activity of Sac1, phosphatase assays were performed on Flag-tagged Sac1 proteins affinity purified from HeLa cells. WT *Drosophila* Sac1 and human SAC1 (SACM1L) exhibited comparable activity *in vitro*, whereas PR *Drosophila* Sac1 had significantly reduced phosphatase activity, but retained some residual activity compared with phosphatase dead (PD) human SAC1 (Fig. S1; see Materials and Methods). Despite being expressed at equivalent levels at 25°C, Flag-tagged Sac1-TS could not be purified in sufficient quantities for phosphatase assays. Together, these data suggest that $Sac1^{ts}$ encodes an unstable protein.

When raised at 18°C (permissive temperature), $Sac1^{ts}$ mutant flies appeared morphologically normal; however, when raised at 23.5°C or 25°C, $Sac1^{ts}$ mutants had reduced viability (adult flies died 1-3 days post-eclosion) and exhibited a rough eye phenotype (Fig. 2). To characterize the eye defect, we performed scanning electron microscopy (SEM) on WT and $Sac1^{ts}$ mutant eyes. Ommatidia from WT (Fig. 2A-C) or from $Sac1^{ts}$ flies raised at 18°C (Fig. 2D-F) were organized in smooth hexagonal arrays with regularly spaced bristles. In contrast, $Sac1^{ts}$ mutants raised at 23.5°C displayed mildly rough eyes with missing or misplaced bristles (Fig. 2G-I). $Sac1^{ts}$ mutants raised at 25°C exhibited a more severe phenotype, including rough eyes with missing bristles, gaps between ommatidia, and abnormal ommatidial shape (Fig. 2J-L). To understand the cellular basis of the observed defects, we used transmission electron microscopy (TEM). In WT ommatidia, 2°/3°pc were well organized, forming a continuous layer between adjacent PR cell clusters (Fig. 2S,T). In contrast, in $Sac1^{ts}$ mutants, 2°/3°pc appeared dysmorphic and discontinuous, resulting in fused ommatidia where cells from adjacent PR clusters were in direct contact (Fig. 2U-X, arrows). These defects were more severe in $Sac1^{ts}$ flies raised at 25°C (Fig. 2W,X, arrows), and were not observed in $Sac1^{ts}$ flies raised at 18°C (not shown).

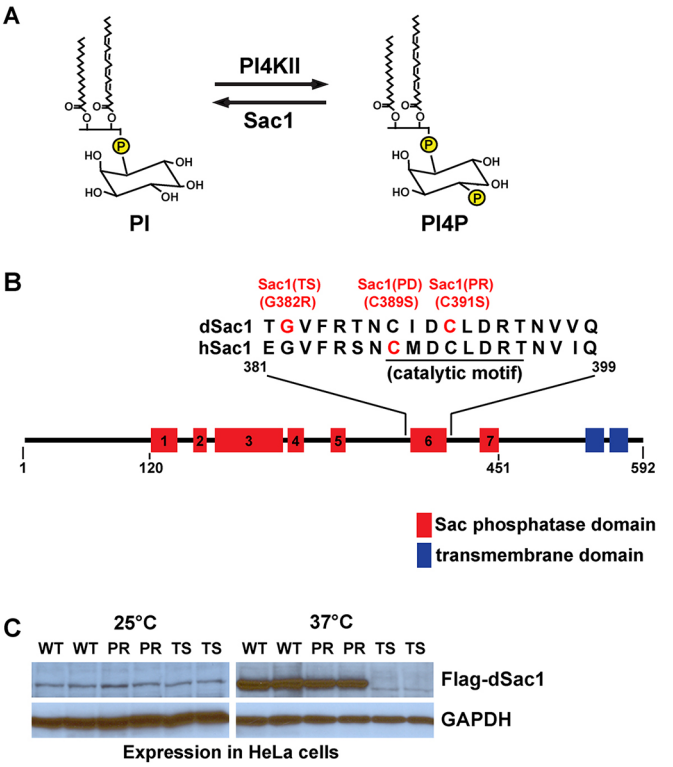

Fig. 1. Sac1 protein is unstable in $Sac1^{ts}$ mutants. (A) Interconversion of PI and PI4P by PI4KII and Sac1. (B) Schematic of Sac1 protein, highlighting conserved domains: Sac domain with conserved motifs (red) and C-terminal transmembrane domains (blue). Sequence alignment of a portion of the Sac domain, including conserved catalytic $CX_5R(T/S)$ motif (underlined), glycine residue mutated in $Sac1^{ts}$ (G382R) (red) and cysteine residues mutated in *Drosophila* Sac1 (dSac1) PR (C391S) and human Sac1 (hSac1) PD (C389S) (red). (C) Immunoblots of lysates from HeLa cells expressing different Flag-tagged dSac1 constructs (WT, PR, TS) at 25°C or 37°C, probed with anti-Flag and anti-GAPDH antibodies (GAPDH, loading control).

To determine whether Sac1 exerts its effect on eye development through regulation of PI4P, we examined genetic interactions with PI4KII (also known as PI4KIIα) (Burgess et al., 2012). By SEM, *PI4KII* null mutants displayed morphologically normal eyes, with the exception of occasional duplicated bristles (Fig. 2M-O). At the ultrastructural level, *PI4KII* mutants showed minor defects in 2°/3°pc morphology (Fig. 2Y,Z); occasionally, PR cells from adjacent ommatidia were in direct contact because of discontinuous 2°/3°pc (Fig. 2Y, arrow). The $Sac1^{ts}$ rough eye phenotype and 2°/3°pc morphology defects, as well as the minor defects in *PI4KII* mutants, were suppressed in $Sac1^{ts}$ *PI4KII* double mutants (Fig. 2P-R,AA, BB), indicating that the two enzymes function antagonistically, consistent with a model in which they regulate a common pool of PI4P important for normal eye development.

Interommatidial cell patterning is highly sensitive to elevated levels of PI4P

To further our understanding of the 2°/3°pc morphology defects in $Sac1^{ts}$ mutants, we examined the adherens junction protein Armadillo (Arm; β-catenin) as a marker for IOC patterning. In WT pupal retinas at 24 h APF, 1°pc were specified and IOCs were uniform and organized single file (Fig. 3A,D,D′). By 30 h

Development (2018) 145, dev151571. doi:10.1242/dev.151571

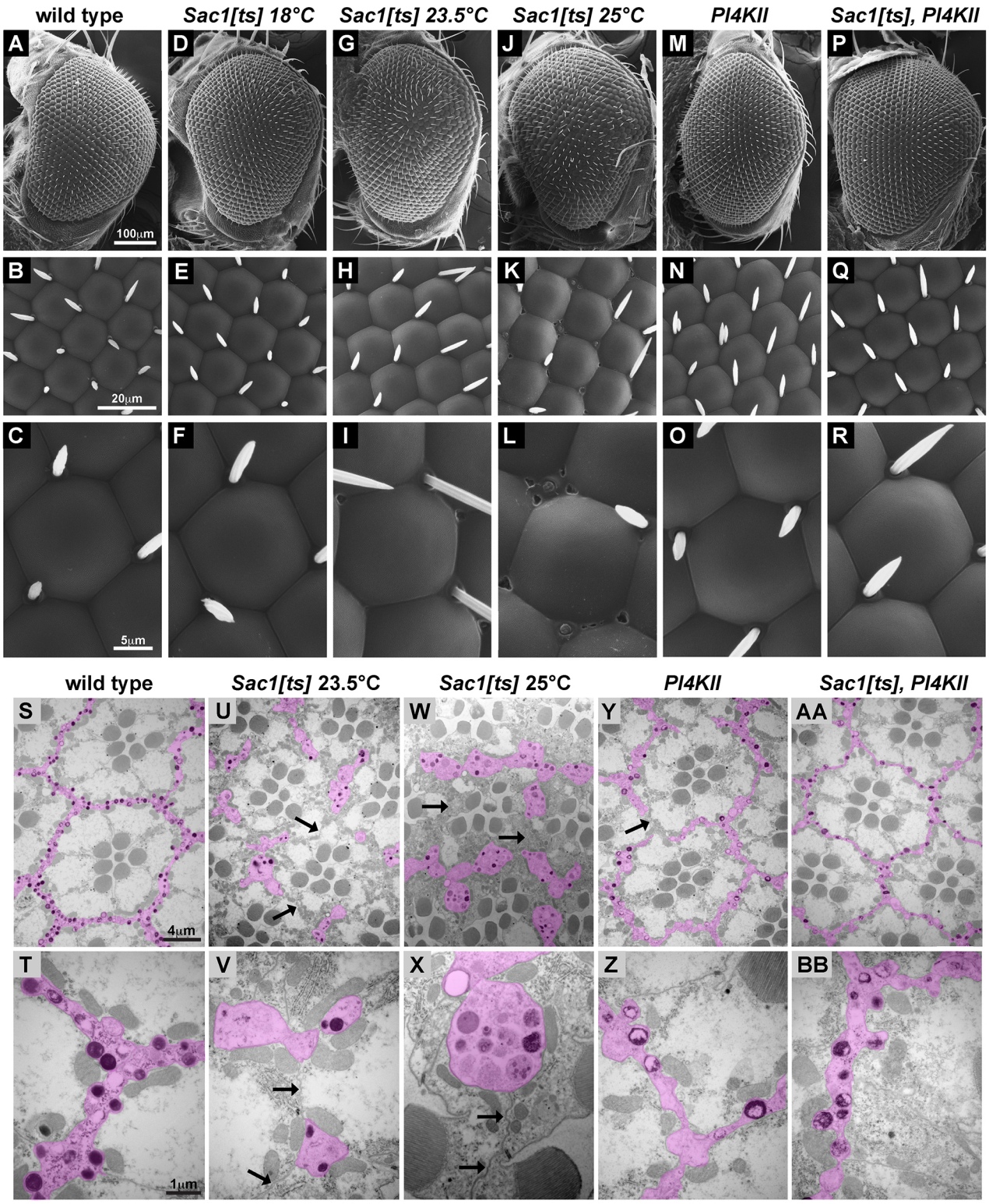

Fig. 2. *Sac1^{ts}* mutants exhibit a rough eye phenotype with defects in pigment cell morphology. (A-R) SEM of 3-day-old adult fly eyes from WT raised at 25°C (A-C), *Sac1^{ts}* raised at 18°C (D-F), *Sac1^{ts}* raised at 23.5°C (G-I), *Sac1^{ts}* raised at 25°C (J-L), *PI4KII* raised at 25°C (M-O) and *Sac1^{ts} PI4KII* raised at 25°C (P-R). (S-BB) TEM of 3-day-old adult fly eyes from WT raised at 25°C (S,T), *Sac1^{ts}* raised at 23.5°C (U,V), *Sac1^{ts}* raised at 25°C (W,X), *PI4KII* raised at 25°C (Y,Z) and *Sac1^{ts} PI4KII* raised at 25°C (AA,BB). Secondary and tertiary pigment cells (2°/3°pc) are pseudocolored. 2°/3°pc discontinuities in *Sac1^{ts}* and *PI4KII* are indicated (U-Y, arrows).

APF, 2°/3°pc began to differentiate and each vertex was occupied by a single cell (Fig. 3B,F,F′). By 42 h APF, cells took on their characteristic shapes and the ommatidial lattice was complete (Fig. 3C,H,H′). At 24 h APF, *Sac1^{ts}* mutant retinas exhibited normal 1°pc; however, IOCs were neither uniform in shape nor organized single file (Fig. 3E,E′, arrow). At 30 h APF, *Sac1^{ts}* IOCs were irregular, bristles were misplaced and multiple cells were present at some vertices (Fig. 3G,G′, arrows). At 42 h APF, the *Sac1^{ts}*

Development (2018) 145, dev151571. doi:10.1242/dev.151571

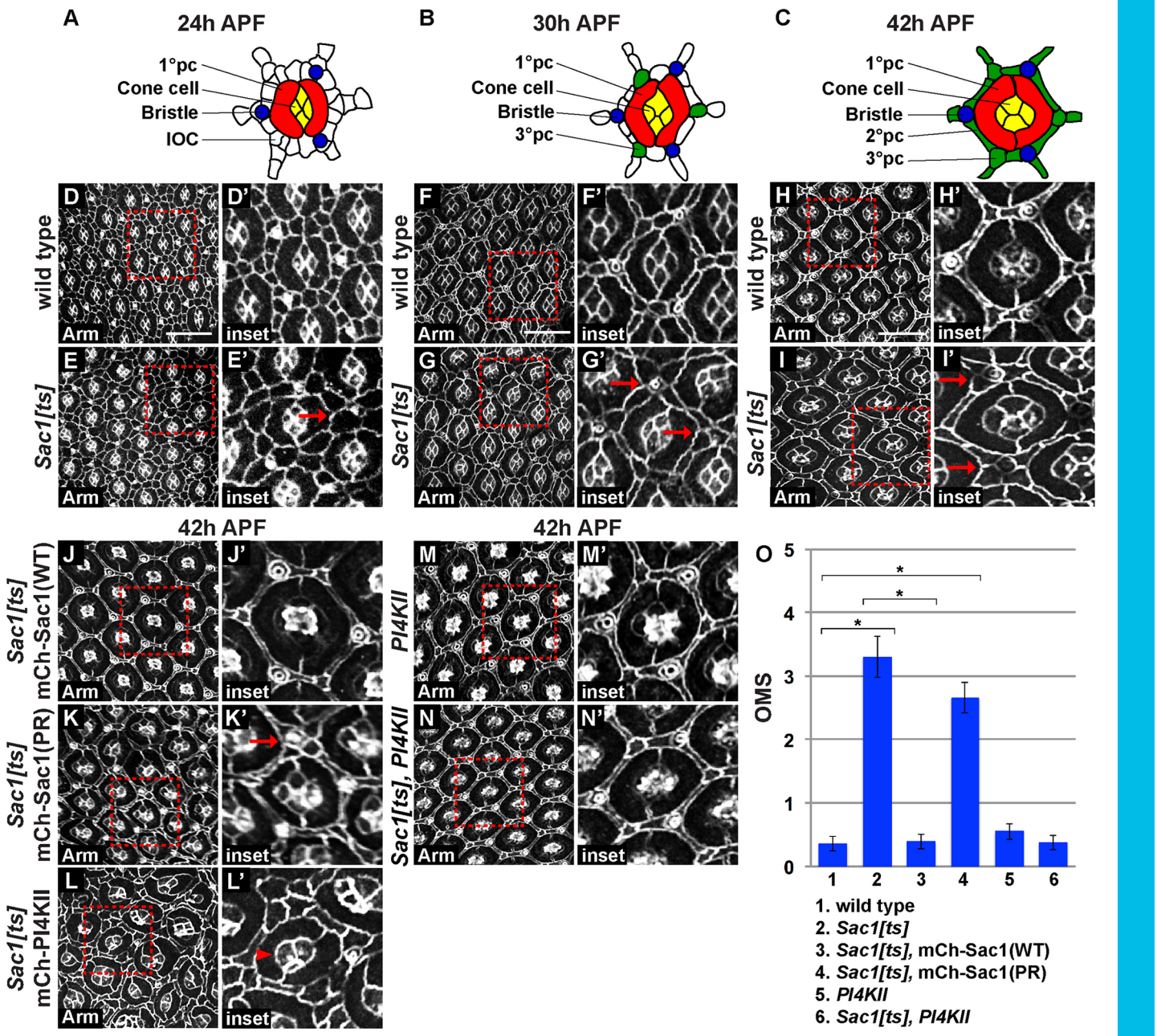

Fig. 3. Sac1 and proper regulation of PI4P are required for IOC patterning. (A-C) Stages of IOC specification in WT pupal retinas at 24 h, 30 h and 42 h APF with 1°pc (red), cone cells (yellow), bristles (blue), IOCs (white), 2°pc (green), 3°pc (green) indicated. (D-N′) Confocal images of pupal retinas stained for Armadillo (Arm, white). Boxed regions (red) in D-N are magnified 2-fold in D′-N′. Note extra cells at some vertices in *Sac1*^{ts} (arrows) and disrupted cone cells in *Sac1*^{ts} expressing mCh-PI4KII (arrowhead). Note that J, M and N show a slightly more basal focal plane. (O) Quantification of ommatidial mispatterning scores (OMS) at 42 h APF for the genotypes listed. n=78 from 3 independent experiments. Error bars represent s.e.m. *P<1×10^{-14}, two-tailed Student's t-test. Scale bars: 15 µm. Flies were raised at 25°C.

ommatidial lattice was disorganized; bristles were disrupted and cells appeared enlarged, with defects in cell number and organization (Fig. 3I,I′, arrows). Discs large (Dlg; Dlg1) staining confirmed the *Sac1*^{ts} IOC patterning defects (Fig. S2). Notably, distribution of Arm and Dlg appeared to be unaffected in *Sac1*^{ts} mutants, indicating that apical junctions were normal. Ommatidial mispatterning scores (OMS) (Johnson and Cagan, 2009) were calculated to quantify the IOC defect (Fig. 3O). WT eyes had an OMS of 0.3±0.11 errors per ommatidium (n=78), whereas *Sac1*^{ts} mutant eyes had a significantly higher OMS of 3.3±0.32 errors per ommatidium (n=78, P<1×10^{-14}). In contrast, *PI4KII* eyes largely resembled WT (Fig. 3M,O; OMS=0.6±0.12, n=78). Hence, Sac1 is required for proper IOC patterning during pupal eye development.

To confirm that the observed defects were due to Sac1 loss of function and increased PI4P levels, we performed rescue experiments and genetic interaction studies. *Sac1*^{ts} IOC patterning defects were rescued by a ubiquitously expressed WT mCherry-Sac1 transgene [mCh-Sac1(WT)] (Fig. 3J,J′,O; OMS=0.4±0.11, n=79), but not by expression of a phosphatase-reduced transgene [mCh-Sac1(PR)] (Fig. 3K,K′,O; OMS=2.7±0.24, n=79). In addition, *Sac1*^{ts} IOC defects were suppressed by *PI4KII* (Fig. 3N,N′,O; OMS=0.4±0.12, n=77) and enhanced by

Development (2018) 145, dev151571. doi:10.1242/dev.151571

expression of mCh-PI4KII (Fig. 3L,L′, arrowhead; OMS not calculated owing to poor survival). Expression of mCh-PI4KII in *Sac1^{ts}* also resulted in abnormal cone cell clusters and disorganized 1°pc (Fig. 3L,L′), which were rarely observed in *Sac1^{ts}* alone (Fig. 3I,I′). Together, these results indicate that the catalytic activity of Sac1 is important for its function in retinal development and suggest that retinal patterning is highly sensitive to elevated levels of PI4P.

To investigate the consequences of the defects in IOC patterning in *Sac1^{ts}*, we examined a previously described reporter line (BA12-lacZ) that provides a readout for 2°/3°pc fate. WT BA12-lacZ flies exhibit nuclear β-gal in 2°/3°pc and bristle cells, as previously described (Araujo et al., 2003), whereas *Sac1^{ts}* BA12-lacZ 2°/3°pc nuclei exhibited reduced β-gal-expression at 42 h APF (Fig. S3). Thus, *Sac1^{ts}* mutants exhibit defects in determining 2°/3°pc fate.

Sac1 affects PIP levels during eye development

To determine whether *Sac1^{ts}* leads to increased PI4P levels *in vivo*, we fused mRFP to the pleckstrin homology (PH) domain of mammalian FAPP1 (PLEKHA3) (mRFP-PH-FAPP), which serves as a coincidence detector that binds Arf1 and PI4P at the Golgi (Dowler et al., 2000; Godi et al., 2004). Compared with WT, *Sac1^{ts}* mutant IOCs displayed increased accumulation of mRFP-PH-FAPP on intracellular organelles (Fig. 4A-B′), with a significant increase in the number (Fig. 4G; n=12, $P<1\times10^{-5}$) and size (Fig. 4H; n=12, $P<1\times10^{-9}$) of PH-FAPP-positive puncta per ommatidium, indicating elevated levels of PI4P. Enlarged PH-FAPP-positive puncta were adjacent to and partially overlapping with the *cis*-Golgi marker Lava lamp (Lva) in *Sac1^{ts}*, suggesting that Sac1 loss resulted in increased Golgi/TGN PI4P (Fig. 4B,B′). A mild but significant increase was observed for the number of Golgi bodies marked by Lva per ommatidium in *Sac1^{ts}* mutants (Fig. 4G; n=12, $P<1\times10^{-3}$); however, the size of Lva-positive puncta was largely unchanged (Fig. 4H).

Sac1 can affect other PIPs in addition to PI4P (Foti et al., 2001; Guo et al., 1999; Nemoto et al., 2000). For example, Sac1 can dephosphorylate PI3P, PI5P and PI(3,5)P_2 *in vitro*. In addition, loss of Sac1 in budding yeast results in reduced levels of PI(4,5)P_2 (Foti et al., 2001; Guo et al., 1999; Hughes et al., 2000). To determine the effect of Sac1 on other PIPs, we examined fluorescent markers for PI3P (mCh-2xFYVE; Gillooly et al., 2000) and PI(4,5)P_2 (PLCδ-PH-GFP; Stauffer et al., 1998; Raucher et al., 2000). mCh-2xFYVE-positive endosomes appeared morphologically similar in WT and *Sac1^{ts}* retinas at 24 h APF (Fig. 4C-D′), indicating that PI3P levels were unaffected in mutant IOCs. In contrast, *Sac1^{ts}* mutants displayed decreased levels of PLCδ-PH-GFP at the IOC PM (Fig. 4E-F′), with the average intensity of PLCδ-PH-GFP at the PM reduced to 70% of WT (Fig. 4I; n=30, $P<1\times10^{-5}$). To quantify the relative defect, we normalized the ratio of PLCδ-PH-GFP to F-actin (Tan et al., 2014), which appeared largely unchanged in *Sac1^{ts}* retinas (Fig. 4F,F′). The PI(4,5)P_2: F-actin ratio was reduced to 67% of WT (Fig. 4J; n=30, $P<1\times10^{-5}$). Together, these data suggest that PI(4,5)P_2 but not PI3P levels are reduced and that PI4P accumulates in the Golgi/TGN of *Sac1^{ts}* IOCs.

Distribution of the IRM protein Rst is sensitive to cold fixation in *Sac1^{ts}*

Because the eye defects in *Sac1^{ts}* mutants resembled mutations in *roughest* (*rst*), we reasoned that Sac1 might regulate localization of Rst or other IRM proteins. To assess the distribution of Rst and its paralog Kirre, we examined WT and *Sac1^{ts}* retinas at 24 h APF by immunofluorescence. In these experiments, fixation was performed on ice to preserve tissue integrity. In WT, Rst and Kirre accumulated at the 1°pc:IOC border, as previously reported (Fig. 5A,A′) (Araujo et al., 2003; Bao et al., 2010; Reiter et al., 1996). However, in *Sac1^{ts}* we observed a dramatic depletion of Rst at the border (Fig. 5B,B′). Quantification of protein intensities at the 1°pc:IOC border revealed a significant decrease in Rst in *Sac1^{ts}* mutants (Fig. 5I; 46% of WT, n=30, $P<1\times10^{-20}$), whereas Kirre showed only a slight decrease (Fig. 5I; 88% of WT, n=30, $P<0.05$).

Rst accumulation at the 1°pc:IOC border requires its binding partner Hbs (Bao and Cagan, 2005; Bao et al., 2010), as well as DE-Cadherin (DE-Cad) (Cordero et al., 2007; Grzeschik and Knust, 2005). To determine whether Rst depletion is a secondary consequence of an effect on these regulators, we examined Hbs and DE-Cad (Shg) at 24 h APF. In *Sac1^{ts}* retinas fixed on ice, Hbs accumulated normally at the 1°pc:IOC border (Fig. 5C-D′,K) and the average ratio of Rst:Hbs at 24 h APF was 47% of WT (Fig. 5L; n=30, $P<1\times10^{-4}$). DE-Cad enrichment at the 1°pc:IOC border was mildly reduced in *Sac1^{ts}* retinas fixed on ice (Fig. 5E-F′,M; 80% of WT, n=30, $P<0.05$). However, the ratio of Rst:DE-Cad was still substantially decreased (Fig. 5N; 65% of WT, n=30, $P<1\times10^{-4}$). Hence, an effect on Hbs or DE-Cad cannot account for the severe defect in Rst accumulation.

At 30 h APF, Kirre, Hbs and DE-Cad all appeared to be unaffected in *Sac1^{ts}*, whereas Rst was still significantly decreased at the 1°pc:IOC border (Fig. S4A-H). Additionally, Notch (another regulator of Rst) (Gorski et al., 2000; Grzeschik and Knust, 2005) was unaffected in *Sac1^{ts}* at 30 h APF (Fig. S4I,J). Thus, the reduction in apical Rst is neither a consequence of disrupting known Rst regulators nor due to a developmental delay in *Sac1^{ts}*.

Surprisingly, in a separate experiment in which retinas were fixed at room temperature (RT), depletion of Rst at the border in *Sac1^{ts}* compared with WT was not observed (Fig. 5G,H). Quantification confirmed that Rst and Kirre intensities at the border were unaffected in *Sac1^{ts}* retinas fixed at RT (Fig. 5O; 95% and 102% of WT, respectively, n=30). The average ratio of Rst:Kirre in *Sac1^{ts}* was 49% of WT when fixed on ice (Fig. 5L; n=30, $P<1\times10^{-20}$), compared with 93% of WT when fixed at RT (Fig. 5P; n=30). The observed difference was not due to sensitivity of the anti-Rst antibody to cold temperature, as only the fixation step was altered (see Materials and Methods). Furthermore, the effect of cold fixation on Rst distribution was specific to *Sac1^{ts}*, as WT retinas fixed on ice or at RT and stained in parallel (i.e. in the same experiment) exhibited no difference in Rst intensity at the 1°pc:IOC border (Fig. S5; n=90).

Although Rst appeared to accumulate normally in *Sac1^{ts}* retinas fixed at RT, it remained possible that the protein could be enriched in secretory vesicles at the cell cortex rather than in the PM. To determine whether Rst is inserted properly at the cell surface in *Sac1^{ts}*, we stained IOCs for exofacial Rst. Retinas at 24-30 h APF were incubated with anti-Rst (which recognizes the extracellular domain) and anti-Lava lamp (Lva, which marks the *cis*-Golgi; a control for membrane permeabilization) prior to RT fixation (see Materials and Methods). Under these conditions, Rst was present at the cell surface in WT and *Sac1^{ts}* retinas and Lva staining was not observed (Fig. S6A-B′). In contrast, both Rst and Lva were detectable upon permeabilization (Fig. S6C-D′). These results demonstrate that Rst is present at the PM in *Sac1^{ts}* following fixation at RT.

To determine whether maintenance of Rst distribution following ice fixation requires Sac1 catalytic activity, we performed rescue experiments. Rst localization in *Sac1^{ts}* tissue fixed on ice was rescued by expression of mCh-Sac1(WT), but not mCh-Sac1(PR) (Fig. 6A-C′). In contrast, Kirre localized to the 1°pc:IOC border

Development (2018) 145, dev151571. doi:10.1242/dev.151571

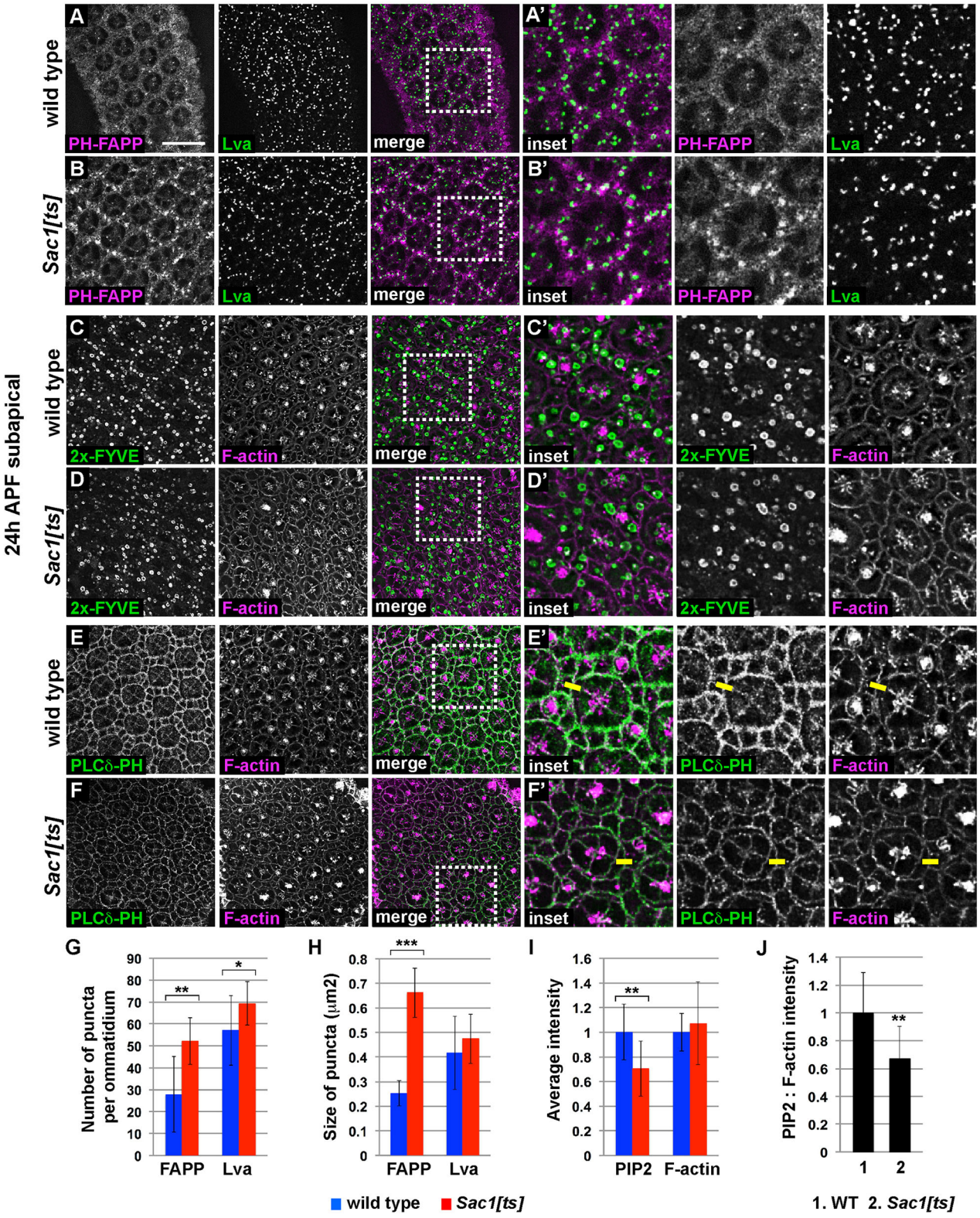

Fig. 4. Loss of Sac1 leads to decreased PI(4,5)P_2 at IOC plasma membranes. (A-B′) Confocal sections of 24 h APF retinas fixed and stained for the PI4P marker mRFP-PH-FAPP (magenta) and the *cis*-Golgi marker Lava lamp (Lva, green). Boxed regions in A,B are magnified 2-fold in A′,B′. (C-F′) Confocal sections of 24 h APF retinas fixed and stained for the PI3P marker mCh-2xFYVE (green, C-D′) or the PI(4,5)P_2 (PIP2) marker PLCδ-PH-GFP (green, E-F′) and F-actin (magenta, C-F′). Boxed regions in C-F are magnified 2-fold in C′-F′. White in merged images indicates colocalization. (G,H) Quantification of number (G) and size (H) of mRFP-PH-FAPP- and Lva-positive puncta. *n*=12 ommatidia from a total of 8 different eyes from 3 independent experiments. (I,J) Quantification of PLCδ-PH-GFP and F-actin intensity at 1°pc:IOC border. Locations of representative line scans are shown (yellow lines in E′,F′). *n*=30 line scans from a total of 10 different eyes from 3 independent experiments. Intensities and ratios normalized to WT. Error bars represent s.d. **P*<1×10^{-3}, ***P*<1×10^{-5}, ****P*<1×10^{-9}, two-tailed Student's *t*-test. Scale bars: 15 µm. Flies were raised at 25°C.

Development (2018) 145, dev151571. doi:10.1242/dev.151571

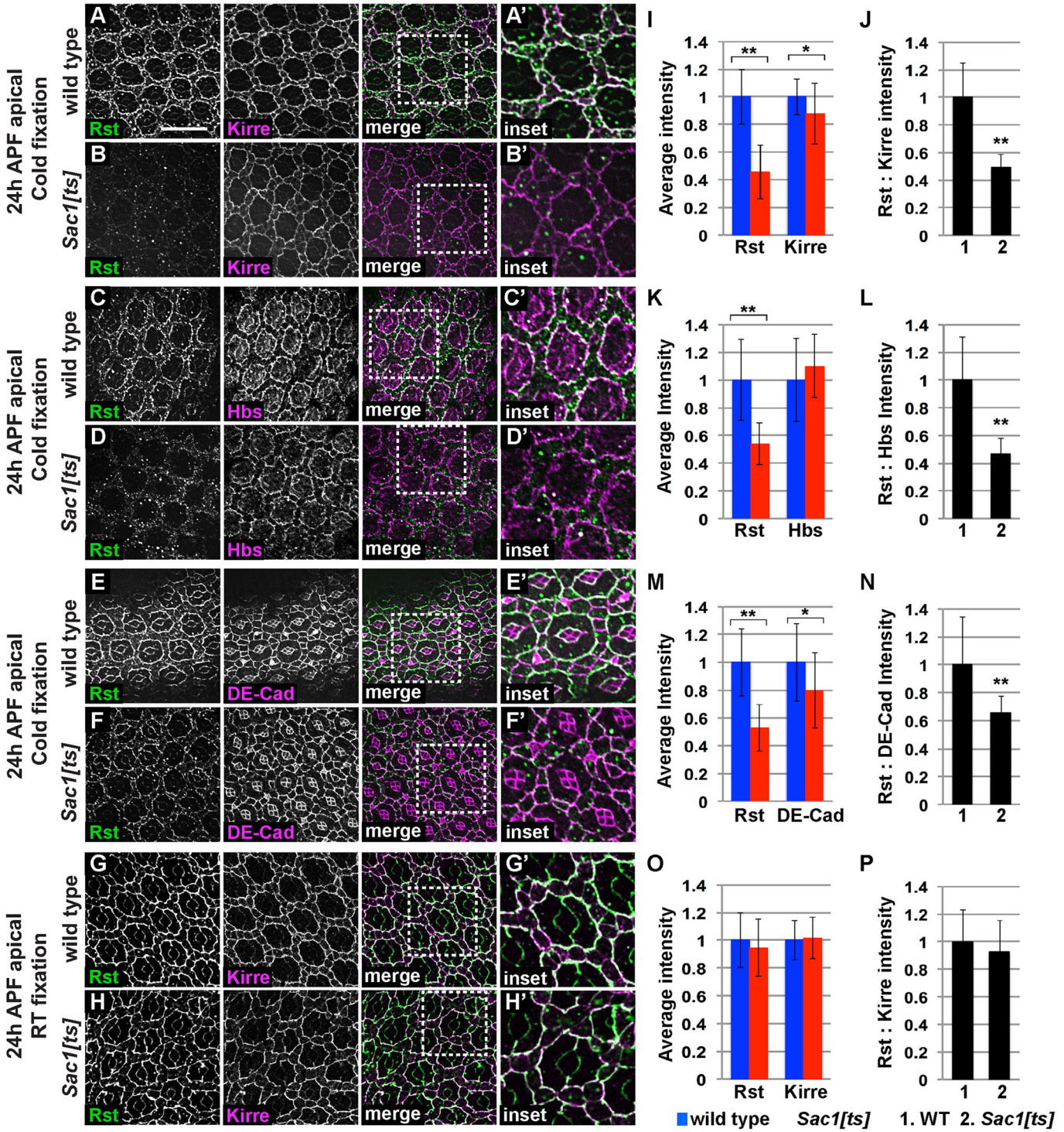

Fig. 5. Rst distribution during retinal patterning is sensitive to cold fixation in *Sac1^{ts}* mutant retinas. (A-H′) Confocal micrographs of 24 h APF retinas (25°C) fixed on ice (cold fixation, A-F′) or at RT (G-H′) and stained for Rst (green) and Kirre (magenta; A-B′,G-H′), Hbs (magenta, C-D′) or DE-Cad (magenta, E-F′). Boxed regions in A-H are magnified 2-fold in A′-H′. White in merged images indicates colocalization. (I-P) Quantification of protein intensities at 1°pc:IOC border. Intensities and ratios are normalized to WT. Error bars represent s.d. n=30 from 3 independent experiments. *P<0.05, **P<1×10^{-20}, two-tailed Student's t-test. Scale bar: 15 µm. Flies were raised at 25°C.

regardless of which transgene was expressed. The average ratio of Rst:Kirre in *Sac1^{ts}* expressing mCh-Sac1(WT) was 103% of WT (n=30, P<0.3), whereas the ratio in *Sac1^{ts}* expressing mCh-Sac1(PR) was 51% of WT (Fig. 6D; n=30, P<1×10^{-6}). Thus, Rst IOC surface localization during incubation in the cold shows a specific sensitivity to loss of Sac1 function not seen with its paralog Kirre.

Sac1 is required for microtubule stability and organization

Mammalian IRM proteins are continuously turned over and replenished at the cell surface by *de novo* synthesis and transport (Satoh et al., 2014). We hypothesized that if turnover occurs in a similar manner in *Drosophila*, loss of Rst at the PM in *Sac1^{ts}* mutants fixed on ice could result from failed replacement of

Development (2018) 145, dev151571. doi:10.1242/dev.151571

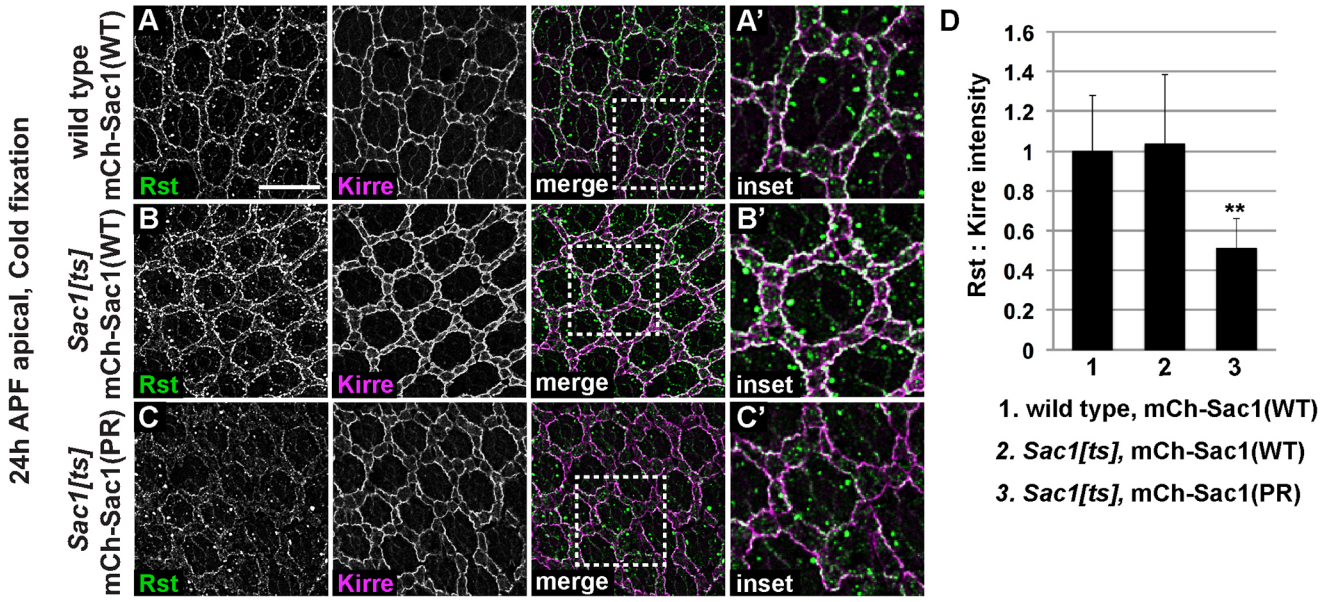

Fig. 6. Catalytic activity of Sac1 is required for Rst maintenance at the plasma membrane. (A-C) Confocal images of pupal retinas at 24 h APF fixed on ice and stained for Rst (green) and Kirre (magenta). White in merged images indicates colocalization. Boxed regions in A-C are magnified twofold in A′-C′. (D) Average intensity ratios of Rst : Kirre at the 1°pc:IOC border. Intensities are normalized to WT. Error bars represent s.d. n=30 from 3 independent experiments. **$P<1\times10^{-6}$, two-tailed Student's t-test. Scale bar: 15 µm. Flies were raised at 25°C.

internalized protein in a cold-sensitive manner. MTs, which are important for vesicle trafficking, are known to be labile under cold conditions (Behnke and Forer, 1967; Roth, 1967; Tilney and Porter, 1967). We stained WT and *Sac1^{ts}* pupal retinas for acetylated α-tubulin and F-actin at 24 h APF. Under both RT (Fig. 7A-B′) and cold (Fig. 7E-F′) fixation conditions, acetylated (stable) MTs were less abundant and appeared disorganized in *Sac1^{ts}* compared with WT. These defects were more pronounced under cold fixation conditions. Line scans across individual IOCs (Fig. 7A′,B′, yellow lines) revealed a significant decrease in the peak intensity of acetylated α-tubulin in *Sac1^{ts}* mutants, whereas the levels and distribution of F-actin were largely unchanged (Fig. 7G; n=30). Similarly, examination of a β-tubulin-GFP transgene revealed a decrease in MT abundance in *Sac1^{ts}* compared with WT following RT fixation (Fig. 7C-D′).

To determine whether Sac1 phosphatase activity is needed for MT stability, pupal retinas from flies expressing mCh-Sac1(WT) or mCh-Sac1(PR) were fixed at RT and stained for acetylated α-tubulin. mCh-Sac1(WT), but not mCh-Sac1(PR), rescued the MT organization defect in *Sac1^{ts}* mutant flies (Fig. 8A-D), confirming that MT stability, abundance and organization in the pupal retina require Sac1 phosphatase activity.

Rst maintenance at the plasma membrane is compromised in *Sac1^{ts}* mutants

To test whether *Sac1^{ts}* mutants fixed on ice have defects in continued delivery of Rst to the PM, we examined localization of the exocyst complex, which is dependent on microtubules in mammalian cells (Vega and Hsu, 2001). WT and *Sac1^{ts}* pupal retinas at 24 h APF were fixed at RT or on ice, and co-stained for Rst and the exocyst subunit Sec8. When prepared at RT, WT and *Sac1^{ts}* pupal retinas exhibited similar staining for Sec8 (Fig. 9A-B′). In subapical regions of the IOCs, we observed small Sec8-positive puncta that showed partial colocalization with Rst. Thus, exocyst-associated trafficking is unperturbed in *Sac1^{ts}* mutants following RT fixation. In contrast, cold fixation resulted in severe defects in Sec8 distribution in *Sac1^{ts}* (Fig. 9D,D′). *Sac1^{ts}* IOCs contained enlarged Sec8-positive structures (>0.3 µm^2) in addition to the small puncta seen in WT (Fig. 9C-D′). Quantification of these structures revealed that WT tissue contained an average of 1.5 enlarged Sec8-positive puncta per ommatidium, whereas *Sac1^{ts}* mutants contained an average of 7.0 (Fig. 9G; n=14, $P<1\times10^{-5}$). In *Sac1^{ts}*, 87% of these enlarged Sec8 structures were positive for Rst (Fig. 9H; n=14). In addition, the percentage of Rst-positive puncta that were positive for Sec8 increased from 3.5% to 24.8% (Fig. 9I; n=14).

To determine whether Rst accumulates in the endocytic pathway, we co-stained for Rst and the late endosome marker YFP-Rab7 in WT and *Sac1^{ts}* retinas fixed on ice. Rst was present in YFP-Rab7-positive endosomes in both WT and *Sac1^{ts}* retinas and no significant difference in colocalization was detected (Fig. 9E-F′). Quantification revealed that although the average number of YFP-Rab7-positive puncta was similar in WT and *Sac1^{ts}* retinas, *Sac1^{ts}* retinas exhibited a significant decrease in the average number of Rst-positive puncta per ommatidium (Fig. 9G).

Taken together, these findings suggest a specific cold-sensitive step in exocyst-dependent trafficking of Rst to the plasma membrane in *Sac1^{ts}*.

To confirm that Rst is internalized upon ice fixation, we performed anti-Rst antibody uptake experiments at 24h APF. In the control experiment, where *Sac1^{ts}* and WT retinas were fixed and permeabilized prior to anti-Lva (as an indicator of permeabilization) and anti-Rst staining, numerous Rst-positive and Lva-positive puncta were observed (Fig. 10A-B′). For antibody uptake, retinas were briefly incubated with anti-Rst and anti-Lva at RT prior to fixation, then washed and fixed on ice (see Materials and Methods). Following this protocol, we observed subapical Rst-positive puncta in IOCs of both *Sac1^{ts}* and WT retinas, with a somewhat higher number in WT (Fig. 10C-D′,I; n=60, P<0.01). Lva staining was not observed, confirming lack of permeabilization during incubation with primary antibodies. When the retinas were incubated for an additional 20 min chase at RT prior to fixation, the number of puncta per ommatidium increased significantly in both WT

Development (2018) 145, dev151571. doi:10.1242/dev.151571

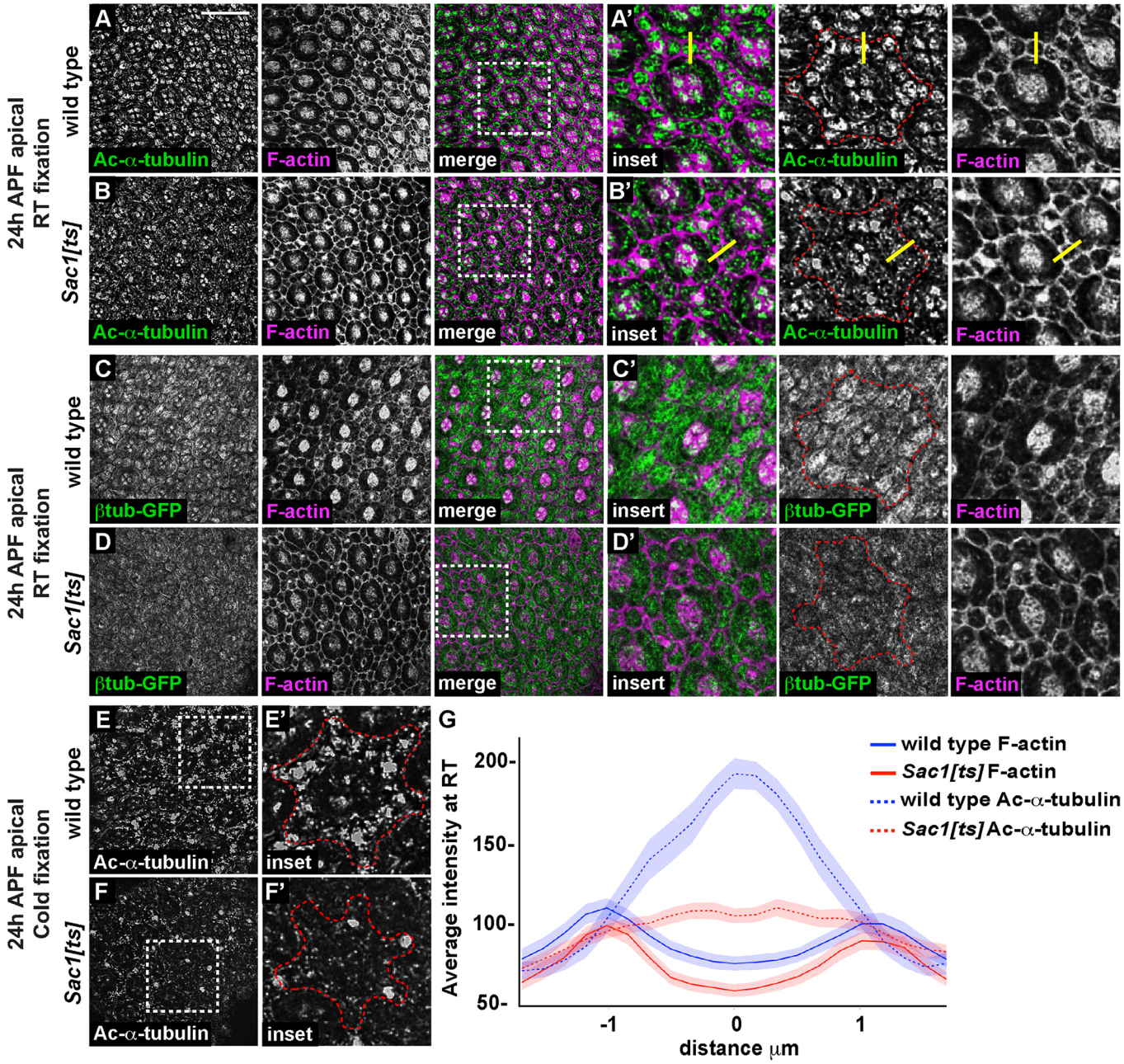

Fig. 7. Sac1 is required for microtubule stability and organization. (A-F′) Confocal micrographs of retinas at 24 h APF fixed at RT (A-D′) or on ice (E-F′). (A-B′,E-F′) Retinas stained for F-actin (magenta in A-B′) and acetylated α-tubulin (green, A-B′; white, E-F′). (C-D′) Retinas from flies expressing β-tubulin-GFP and stained for GFP (green) and F-actin (magenta). Boxed regions in A-F are magnified 2-fold in A′-F′. White in merged images indicates colocalization. Red dashed lines in acetylated α-tubulin inset panels outline single ommatidia. (G) Graph showing average line intensity scans across WT (blue) or *Sac1*^{ts} (red) IOCs stained for acetylated α-tubulin (dashed lines) and F-actin (solid lines) under RT fixation conditions. Zero on the *x*-axis marks the cell center. Shading represents s.e.m. Locations of representative line scans are shown (yellow lines in A′,B′). *n*=30 scans from a total of 15 different eyes from 3 independent experiments. Scale bar: 15 µm. Flies were raised at 25°C.

(Fig. 10E,E′; n=60, $P<1\times10^{-6}$) and *Sac1*^{ts} (Fig. 10F,F′; n=60, $P<1\times10^{-12}$), to roughly similar levels (Fig. 10I). Together, these results indicate that Rst is internalized from the plasma membrane in retinas fixed on ice, and that Rst turnover occurs *ex vivo* prior to fixation. In addition, when retinas were co-stained with anti-Sec8 following anti-Rst uptake and cold fixation (see Materials and Methods), instances of colocalization were observed in both *Sac1*^{ts} and WT, suggesting endocytosed Rst is partially recycled to the plasma membrane via an exocyst-mediated pathway (Fig. 10G-H′).

DISCUSSION

Conditional alleles are powerful tools for studying the functions of essential genes. Here, using a temperature-sensitive allele of *Sac1*, we show that proper phospholipid regulation by Sac1 is required for normal development of the *Drosophila* retinal epithelium.

Our results indicate that retinal patterning is highly sensitive to elevated levels of PI4P. Loss of Sac1 leads to increased Golgi PI4P and IOC patterning defects that are rescued by expression of catalytically active Sac1. Deletion of *PI4KII* suppresses *Sac1*^{ts}, whereas expression of a WT PI4KII transgene exacerbates the observed defects. Thus,

Development (2018) 145, dev151571. doi:10.1242/dev.151571

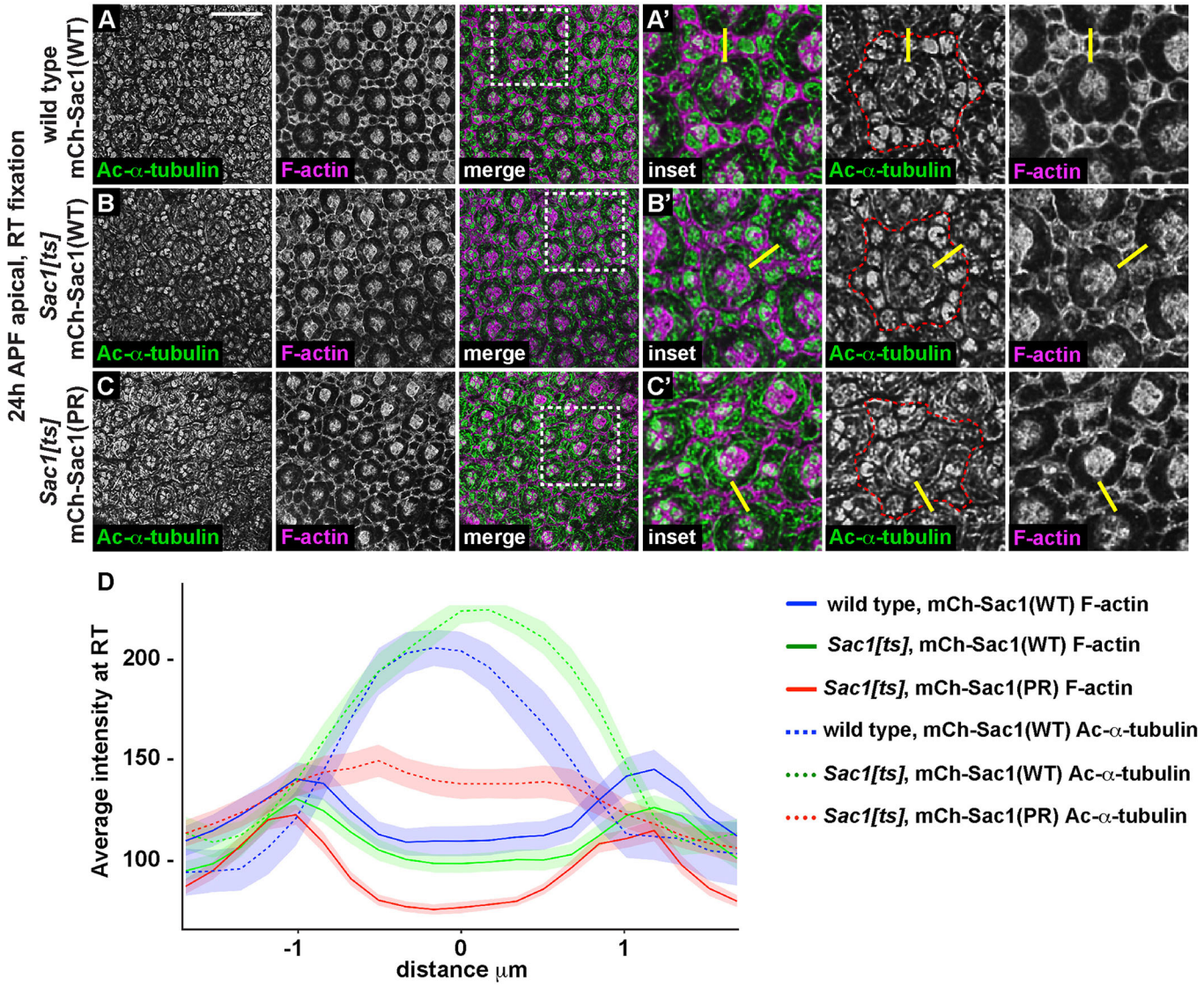

Fig. 8. Catalytic activity of Sac1 is required for microtubule stability and organization. (A-C′) Confocal images of pupal retinas at 24 h APF fixed at RT and stained for acetylated α-tubulin (green) and F-actin (magenta). White in merged images indicates colocalization. Red dashed lines in acetylated α-tubulin inset panels outline single ommatidia. (D) Graph showing average line intensity scans across WT (blue), *Sac1*^{ts} expressing mCh-Sac1(WT) (green) or *Sac1*^{ts} expressing mCh-Sac1(PR) (red) IOCs stained for acetylated α-tubulin (dashed lines) and F-actin (solid lines). Zero on the *x*-axis marks the cell center. Shading represents s.e.m. Locations of representative line scans are shown (yellow lines in A′-C′). *n*=30 from 3 independent experiments. Scale bar: 15 µm. Flies were raised at 25°C.

Sac1 and PI4KII regulate a pool of PI4P that is required for retinal patterning. Loss of *PI4KII* itself results in mild patterning defects (i.e. occasional extra bristles and fused ommatidia), indicating that reducing PI4P levels also has consequences for retinal development. Although these data point to a clear role for PI4KII in signaling required for 2°/3°pc adhesion and patterning, our experiments do not rule out possible contributions of other PI4Ks to this process. Moreover, we anticipate that, in addition to the Golgi, other pools of PI4P at the PM (Cheong et al., 2010; Faulhammer et al., 2005; Manford et al., 2012; Roy and Levine, 2004; Tahirovic et al., 2005) and elsewhere (Hammond et al., 2014) may be regulated by Sac1.

Because PI4P is phosphorylated by PIP 5-kinases to produce $PI(4,5)P_2$, *Sac1*^{ts} mutants might be expected to show increased levels of $PI(4,5)P_2$ as well as PI4P. Strikingly, however, we found that *Sac1*^{ts} mutants exhibit reduced levels of the $PI(4,5)P_2$ marker PLCδ-PH at the PM. Although this result is counterintuitive, similar observations have been reported in budding yeast (Foti et al., 2001; Guo et al., 1999; Hughes et al., 2000), and we previously observed the same phenomenon in *Drosophila* embryos homozygous for a lethal allele of *Sac1* (unpublished data). We note that this observation is in contrast to other *Drosophila* tissues, where Sac1 loss was reported to have no effect on $PI(4,5)P_2$ levels (Forrest et al., 2013; Yavari et al., 2010). It is possible that PIP 5-kinases lack access to the increased PI4P in *Sac1* mutants, thereby preventing the expected increase in $PI(4,5)P_2$, or perhaps increased PI4P triggers a feedback mechanism that activates PIP phosphatases or phospholipases, leading to $PI(4,5)P_2$ breakdown. Thus, in addition to elevated PI4P levels, reduced levels of $PI(4,5)P_2$ might contribute to the IOC patterning defects in *Sac1*^{ts}. Indeed, in preliminary results we observed a genetic interaction between *Sac1* and the PI4P 5-kinase *skittles* (not shown), which could stem from reduced $PI(4,5)P_2$ or increased PI4P levels, or a combination of the two.

Development (2018) 145, dev151571. doi:10.1242/dev.151571

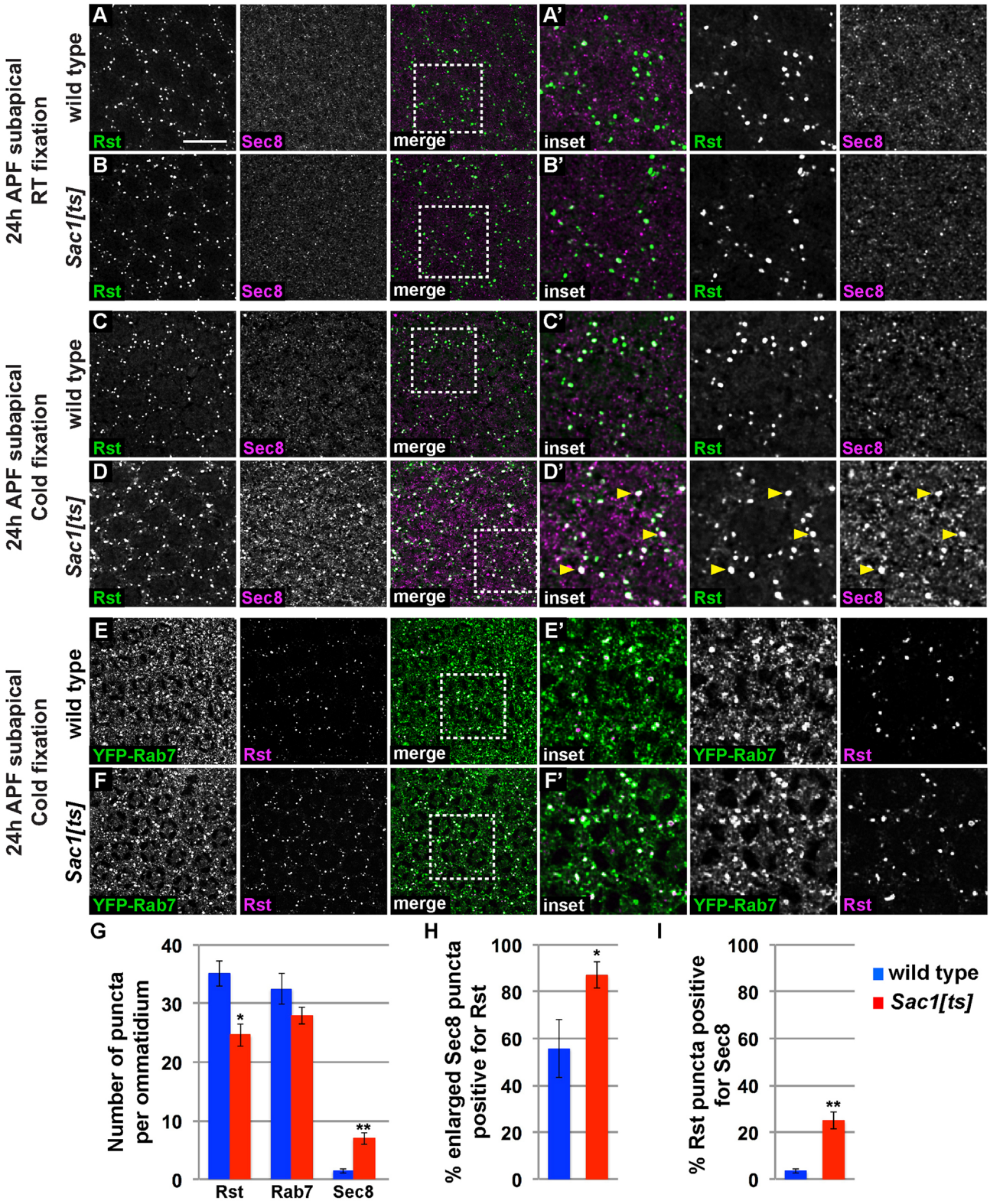

Fig. 9. Rst and Sec8 accumulate in enlarged structures in *Sac1^{ts}* retinas incubated in the cold. (A-D) Subapical confocal sections of retinas at 24 h APF stained for Rst (green) and Sec8 (magenta). Retinas were fixed at RT (A-B′) or on ice (C-D′). (E-F′) Subapical confocal sections of retinas expressing YFP-Rab7. Retinas were dissected at 24 h APF, fixed on ice and stained for YFP (green) and Rst (magenta). White in merged images indicates colocalization. Arrowheads in D′ indicate enlarged Sec8-positive puncta that contain Rst. (G-I) Quantification of Rst-, Rab7- and Sec8-positive puncta in WT and *Sac1^{ts}* samples fixed on ice. (G) Average number of Rst-, Rab7- and enlarged Sec8-positive puncta per ommatidium. The percentage of enlarged Sec8-positive puncta that contain Rst (H) and the percentage of Rst-positive puncta that contain Sec8 (I) are increased in *Sac1^{ts}*, compared with WT. Boxed regions in A-F are magnified 2-fold in A′-F′. Error bars represent s.e.m. n=14 ommatidia from a total of 7 different eyes from 3 independent experiments. *P<0.05, **P<1×10^{-5}, two-tailed Student's t-test. Scale bar: 15 µm. Flies were raised at 25°C.

Development (2018) 145, dev151571. doi:10.1242/dev.151571

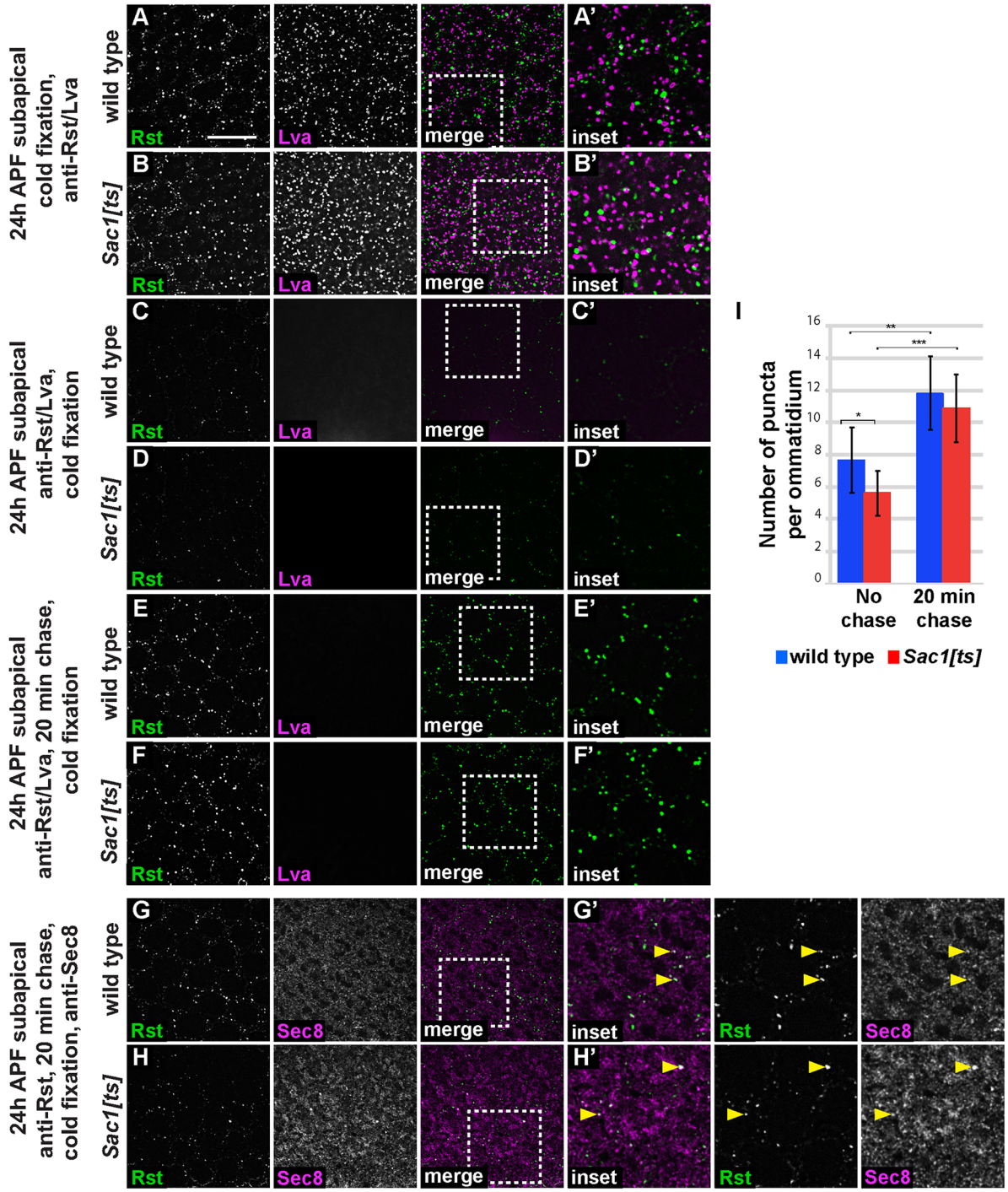

Fig. 10. Uptake of anti-Rst antibody occurs in WT and *Sac1^{ts}* retinas. (A-F′) Subapical confocal sections of retinas at 24 h APF stained for Rst (green) and Lva (magenta). (A-B′) Retinas were dissected at 24 h APF, fixed on ice, permeabilized, and stained for Rst and Lva. (C-D′) Retinas were dissected at 24 h APF, incubated for 10 min in anti-Rst/anti-Lva primary antibodies, washed, fixed on ice, permeabilized, and stained with fluorescently conjugated secondary antibodies. (E-F′) As in C-D′, except retinas were incubated for 10 min in anti-Rst/anti-Lva primary antibodies, washed, and kept at RT for 20 additional minutes (chase) prior to fixation. (G-H′) Subapical confocal sections of retinas at 24 h APF stained for Rst (green) and Sec8 (magenta). Retinas were dissected at 24 h APF, incubated in anti-Rst primary antibody for 10 min, washed and kept at RT for an additional 20 min (chase), fixed on ice, permeabilized, incubated in anti-Sec8 primary antibody, washed and stained with fluorescently conjugated secondary antibodies. Arrowheads in G′,H′ indicate colocalization. Boxed regions in A-H are magnified 2-fold in A′-H′. White in merged images indicates colocalization. (I) Average number of Rst-positive puncta (>0.1 μm^2) per ommatidium. Error bars represent s.d. *n*=60 ommatidia from a total of 20 different eyes from 3 independent experiments. **P*<0.01, ***P*<1×10^{-6}, ****P*<1×10^{-12}, two-tailed Student's *t*-test. Scale bar: 15 μm. Flies were raised at 25°C.

Drosophila Sac1^{ts} mutants exhibit rough eyes, ommatidial mispatterning and abnormal 2°/3°pc morphology, phenotypes that resemble mutants for the IRM protein Rst. Maintenance of Rst at the 1°pc:IOC border is sensitive to ice fixation in *Sac1^{ts}* mutant retinas. Because MTs are labile under cold conditions, this suggested a MT defect in *Sac1^{ts}*. MTs are disorganized in *Sac1^{ts}* mutant IOCs fixed

Development (2018) 145, dev151571. doi:10.1242/dev.151571

at RT, and even more dramatically affected in mutant IOCs fixed on ice. Moreover, *Sac1^{ts}* IOCs fixed on ice display enlarged Sec8-positive vesicles containing Rst, suggesting that Rst travels to the cell surface via an exocyst- and MT-associated pathway that is sensitive to cold fixation in *Sac1^{ts}*.

The simplest model to explain our data is that Rst is constantly turned over at the PM and requires continuous replenishment from internal stores, as has been reported for mammalian IRM proteins (Satoh et al., 2014). This turnover appears to occur in both WT and *Sac1^{ts}*, as we observed similar uptake of anti-Rst antibody in each. It remains possible that subtle defects in the activity or turnover of Rst (or other proteins) at the PM contribute to the observed defects in *Sac1^{ts}*. Indeed, we observed compromised expression of the differentiation marker BA12-lacZ in *Sac1^{ts}* IOCs. Defects in BA12-lacZ expression, as well as IOC number and specification, also occur in *Rst^{D}* mutants, which show a delay in Rst accumulation at the 1°pc:IOC border (Araujo et al., 2003). Relevant to this point, we note that when quantification of Rst distribution after RT or cold fixation was independently validated at a later date, we observed a slight but significant reduction in Rst accumulation in *Sac1^{ts}* following RT fixation (84% of WT; n=90). However, as this difference was not observed in our earlier experiments (Fig. 5G,H, O), we are unable to conclude that there is a reproducibly significant decrease in Rst accumulation in *Sac1^{ts}*.

Sac1 was originally identified as a suppressor of yeast actin mutants (Cleves et al., 1989; Novick et al., 1989). Thus, much of the literature has focused on how Sac1 loss affects the actin cytoskeleton. Here, we observed that retinal cells in *Drosophila Sac1^{ts}* mutants exhibit normal actin organization during early stages of pupal eye development (24-30 h APF), yet show defects in MT stability and organization. Interestingly, both increased levels of PI4P and reduced levels of PI(4,5)P_2 have previously been associated with defects in MT organization (Forrest et al., 2013; Gervais et al., 2008; Liu et al., 2009; Wei et al., 2008). The molecular mechanisms involved remain unknown, and further investigation will be required to determine the link between Sac1 and MT stability. However, our observations suggest that regulation of the MT cytoskeleton by Sac1 may be more important when moving from fungal to animal models.

In summary, we have characterized a requirement for Sac1 in maintaining PI4P and PI(4,5)P_2 levels and promoting normal development of the *Drosophila* retina. Additionally, we have demonstrated that Rst distribution in *Sac1^{ts}* is sensitive to cold fixation, and that *Sac1^{ts}* exhibits a microtubule defect at 24 h APF. Our results indicate that Rst is delivered to the PM via exocyst- and microtubule-based trafficking (which is cold sensitive in *Sac1^{ts}*) and is turned over at the PM, similar to its mammalian homologs. Further investigation will be required to unravel precisely how Sac1 regulates microtubules, and how this contributes to normal retinal development.

MATERIALS AND METHODS

Fly stocks and genetic crosses

Flies were raised on standard cornmeal molasses agar (Ashburner, 1990). Crosses and staging were performed at 25°C unless otherwise indicated. Stocks were Oregon R (wild type, WT), *w^{+}; Sco/CyO; FRT80B, Sac1^{ts}* (*Sac1^{ts}*, previously known as *l(3)2107* or *sac1^{L4H}*) (Wei et al., 2003b), *w^{+}; Sco/CyO; P{w^{+}, CG14671}, P{neoFRT}82B, Df(3R)730* (*PI4KII*) (Burgess et al., 2012) and *w^{+}; Sco/CyO; Sac1^{ts}, P{w^{+}, CG14671}, P{neoFRT}82, Df(3R)730* (*Sac1^{ts} PI4KII*) (this work). The following transgenes on chromosome II were crossed into the *Sac1^{ts}* mutant background: *P{w^{+},* α_1-tubulin::*mCherry-PI4KII}* (Burgess et al., 2012), *P{w^{+},* α_1-tubulin::*mCherry-Sac1(WT)}* (WT Sac1) and *P{w^{+},* α_1-tubulin::*mCherry-Sac1(PR)}* [phosphatase reduced (PR) Sac1] (this study). Additional stocks were *w, BA12-lacZ* (gift of R. Ramos, University of São Paulo, Brazil) (Araujo et al., 2003), *w; P{w^{+}, UAS-mRFP-PH-FAPP}/CyO* (this study), *w; P{w^{+}, UAS-mCherry-2xFYVE}* (gift of A. Kiger, UCSD, CA, USA) (Velichkova et al., 2010), *w; P{w^{+}, UAS-PLCδ-PH-GFP}/CyO* (gift of L. Cooley, Yale University, CT, USA) (von Stein et al., 2005), *P{w^{+}, YFP-Rab7}* (gift of S. Eaton, Dresden, Germany) (Marois et al., 2006), *w; P{w^{+}, β-tub-GFP}/CyO* (gift of Y. Akiyama-Oda and H. Oda, JT Biohistory Research Hall, Takatsuki City, Japan) (Inoue et al., 2004) and *y^{1} w*; P{Act5C-GAL4}25FO1/CyO* (to drive expression of *UAS-mRFP1-PH-FAPP*, *UAS-mCherry-2xFYVE* and *UAS-PLCδ-PH-GFP*; Bloomington *Drosophila* Stock Center, IN, USA).

Molecular biology

To generate *Drosophila* Sac1 constructs for expression in cultured mammalian cells, WT Sac1 was amplified from cDNA (GH08349, BDGP, Berkeley, CA, USA) and a Flag tag was added to the 5′ end using standard molecular techniques; Flag-Sac1 was amplified using primers 5′-GCGGTACCATGGACTACAAGGACGACGATGACAAGATGGACAG-CAGGGAGGAGAACGCC-3′ and 5′-GCTCTAGATCATGGGTCTCGA-AAGGAGATGGG-3′ (Invitrogen) and cloned into the mammalian expression vector pCDNA3.1 with *Asp718* and *Xho*I. Phosphatase reduced (PR, C391S) and temperature sensitive (TS, G382R) mutations were introduced using QuikChange XL (Stratagene). Flag-Sac1[PR] and Flag-Sac1[TS] were generated using the mutagenesis primers 5′-GAACG-AATTGTATCGACTCTCTCGATAGGACGAACGTCGCGACGTTCGT-CCTATCGAGAGAGTCGATACAATTCGTTC-3′ and 5′-GTCCACGC-AGACTCGTGTCTTCCGAACGAATTGCAATTCGTTCGGAAGACAC-GAGTCTGCGTGGAC-3′, respectively (Invitrogen). Note that although the mutated cysteine in *Drosophila* Sac1(PR) is conserved and present in the catalytic motif (C391), it is not the same residue that is mutated in phosphatase dead (PD, C389S) human SAC1 (Rohde et al., 2003), likely explaining the residual phosphatase activity.

To generate transgenic flies, Sac1(WT) and Sac1(PR) were subcloned from pCDNA3.1 into a modified pCaSpeR4 vector containing the α*Tub84B* promoter (α_1-*tubulin*) fused to *mCherry* (Goldbach et al., 2010) using *Kpn*I and *Xba*I. mRFP1-PH-FAPP was amplified from tv3::mRFP-PH-FAPP (Wei et al., 2008) using standard molecular techniques and subcloned into pUAST (Brand and Perrimon, 1993) with *Not*I and *Asp718*. Transgenic lines carrying pUAST::mRFP-PH-FAPP were generated in the lab. All other transgenic lines were made by BestGene using standard P-element transformation techniques.

Scanning electron microscopy

For SEM, heads from 3-day-old flies were bisected and fixed in 2% glutaraldehyde in 0.1 M sodium cacodylate buffer for 2 h. Samples were rinsed with 0.1 M sodium cacodylate buffer in 0.2 M sucrose for 20 min and dehydrated in an ethanol series of 20 min washes. After dehydration, samples were subjected to critical-point drying (Bal-Tec CPD 030 Critical Point Dryer), attached to an aluminum stub, and sputter-coated with gold (Denton Desk II sputter coater) (Advanced Bioimaging Center, Mount Sinai Hospital, Toronto, Canada). Samples were imaged using a Phillips/FEI XL30 scanning electron microscope. Images were uniformly edited with Adobe Photoshop CS6.

Transmission electron microscopy

Fly eyes were prepared for TEM as described (Pellikka et al., 2002). In brief, heads from 3-day-old flies were immobilized in PBS, bisected and fixed in 1% OsO_4 in 0.1 M cacodylate buffer. Samples were left in fixative for 3 days on a nutator at 4°C. Samples were washed with 0.1 M cacodylate buffer, placed in fixative in the dark for 1 h, washed again with 0.1 M cacodylate buffer, dehydrated in an ethanol series (50%, 70%, 80%, 90% and 100% for 5 min each), embedded in fresh Spurr's resin and polymerized in rubber molds at 65°C for 8 h. Embedded samples were sectioned (Reichert Ultracut E ultramicrotome) and imaged at 5000× or 19,000× using a FEI Tecnai 20 transmission electron microscope and AMT digital camera (Advanced Bioimaging Center, Mount Sinai Hospital, Toronto, Canada). Images were uniformly edited with Adobe Photoshop CS6.

Development (2018) 145, dev151571. doi:10.1242/dev.151571

Cell culture and protein analysis

HeLa cells (ATCC HeLa 229 cell line, Manassas), which were authenticated and tested for contamination, were grown in DMEM (Sigma-Aldrich) supplemented with 10% fetal bovine serum. Cells were maintained at 37°C in a humidified atmosphere with 5% CO_2. Cells were seeded on culture plates 24 h before transfection. Cells were transfected with plasmids for transient expression of Flag-tagged *Drosophila* (this study) or human (Rohde et al., 2003) Sac1 constructs using Lipofectamine 2000 (Invitrogen). Transfected cells were kept for 4 h at 37°C and then further incubated for 18 h at either 37°C or 25°C. Cells were lysed in mRIPA buffer (1% NP-40, 1% sodium deoxycholate, 150 mM NaCl, 50 mM Tris-HCl, pH 8.0) supplemented with protease inhibitor cocktail (Roche). Flag-tagged Sac1 proteins were analyzed by SDS page and immunoblotting (1:1000) using mouse monoclonal anti-Flag M2 antiserum (Sigma-Aldrich F3165). Anti-GAPDH antibody (1:1000; Abcam, ab9485) was used as the loading control.

Phosphatase assays

HeLa cells were transfected as above with plasmids for transient expression of Flag-tagged Sac1. Two days after infection, cells were washed once with PBS and lysed in mRIPA buffer supplemented with protease inhibitor cocktail (Roche). Following centrifugation at 13,000 ***g*** for 15 min, Flag-tagged Sac1 proteins were collected on M2 agarose beads. A modified version of a published protocol (Blagoveshchenskaya et al., 2008) was used to measure phosphatase activity: 24 µl of reaction buffer (200 mM sodium acetate, 100 mM Bis-Tris, 100 mM Tris, pH 6.0, 0.002% porcine gelatin and 4 mM DTT), 1.4 µl of 1 M dioctanoyl-PI4P in water (Sigma-Aldrich) and M2 agarose beads containing 4 µg of recombinant Sac1 protein were mixed and incubated at 37°C for various times. Reactions were stopped by addition of an equal volume of 100 mM NEM and 25 µl of each supernatant was pipetted into 96-well plates. 50 µl of Malachite Green solution (1 volume 4.2% ammonium molybdate in 4 M HCl, 3 volumes of 0.045% Malachite Green and 0.01% Tween 20) was added to each well. After incubation for 20 min at RT, OD_{620} was measured.

Immunocytochemistry

Pupal eyes were dissected in PBS as described (Walther and Pichaud, 2006) and fixed in 4% paraformaldehyde (PFA) for 30 min. Fixation was performed on ice, unless otherwise stated. After fixation, samples were washed in PBS containing 0.3% saponin (PBSS), blocked in PBSS with 5% normal goat serum (NGS) for 1 h at RT, and incubated with primary antibodies in PBSS with 5% NGS overnight at 4°C. Samples were washed and incubated with secondary antibodies in PBSS with 10% NGS. DE-Cad staining was as described above, except phosphate buffer was used instead of PBS. Rhodamine-conjugated phalloidin was used at 4 U/ml to visualize F-actin (Invitrogen). DAPI (Thermo Fisher Scientific, D1306) was used at 1:1000 to stain DNA. Samples were mounted in Dako fluorescence mounting medium (Agilent Technologies).

Primary antibodies were mouse anti-acetylated α-tubulin 6-11B (Sigma-Aldrich, T7451, 1:1000), mouse anti-Arm N2 7A1 [Developmental Studies Hybridoma Bank (DSHB), AB_528089, 1:150] (Riggleman et al., 1990), mouse anti-β-gal (Promega, Z3781, 1:250), rat anti-DE-Cadherin DCAD2 (DSHB, AB_528120, 1:50) (Oda et al., 1994), mouse anti-Dlg 4F3 (DSHB, AB_528203, 1:500) (Parnas et al., 2001), rat anti-dsRed (ChromoTek, 5f8-100, 1:500), mouse anti-GFP 3E6 (Life Technologies, A-11120, 1:500), chicken anti-GFP (Abcam, 13970, 13970, 1:500), rabbit anti-Hibris AS14 (from Karl-Friedrich Fischbach, 1:300) (Bao et al., 2010), rabbit anti-Kirre (from Karl-Friedrich Fischbach, 1:300), rabbit anti-Lava lamp (gift of J. Sisson and O. Papoulas, 1:1000) (Sisson et al., 2000), mouse anti-Notch^{ICD} C17.9C6 (DSHB, AB_528410, 1:500) (Fehon et al., 1990), mouse anti-Roughest mAb24A5.1 (from Karl-Friedrich Fischbach, 1:50) (Schneider et al., 1995), guinea pig anti-Sec8 (gift of U. Tepass, 1:1000) (Beronja et al., 2005), Secondary antibodies conjugated to Alexa 488, 568 or 633 were used at 1:500 (Molecular Probes, Life Technologies).

Staining for exofacial Rst

Pupal eyes were dissected in PBS as described (Walther and Pichaud, 2006), kept at RT, and stained according to one of two methods. For no permeabilization, tissue was incubated with anti-Rst and anti-Lva in PBS containing 5% NGS for 1 h prior to fixation in 4% PFA for 30 min. For permeabilization, tissue was fixed in 2% PFA for 30 min and then incubated with anti-Rst and anti-Lva in PBS containing 5% NGS for 1 h. In either case, samples were then washed, incubated with secondary antibodies in PBS containing 5% NGS, washed again, and mounted for imaging.

Rst uptake assay

Pupal eyes were dissected in Schneider's media (1% fetal bovine serum) as described (Walther and Pichaud, 2006), and stained according to one of three methods. For permeabilization control, tissue was fixed on ice in 4% PFA for 30 min, washed in PBSS for permeabilization, and incubated with anti-Rst and anti-Lva in PBS containing 5% NGS for 10 min. For antibody uptake (no chase), tissue was incubated in anti-Rst and anti-Lva in Schneider's media (1% fetal bovine serum) containing 5% NGS for 10 min, washed in PBS, and then fixed on ice in 4% PFA for 30 min and washed in PBS. For antibody uptake (with chase), tissue was incubated in anti-Rst and anti-Lva in Schneider's media (1% fetal bovine serum) containing 5% NGS for 10 min, washed in Schneider's media, incubated for 20 min at RT, washed in PBS, and then fixed on ice in 4% PFA for 30 min, and washed in PBS. In all cases, samples were then washed in PBSS for permeabilization, blocked in PBSS with 5% NGS for 1 h, incubated with secondary antibodies in PBSS containing 10% NGS, washed again, and mounted for imaging in ProLong Diamond Antifade Mountant (Thermo Fisher).

Confocal imaging and analysis

Images were acquired on a Quorum spinning disk confocal microscope featuring the following components: Yokogawa CSU-X1 scanhead, Olympus IX81 microscope, 60×/1.35 oil-immersion objective, Spectral Applied Research laser merge module (excitation wavelengths: 405 nm, 491 nm, 561 nm, 640 nm) and Hamamatsu C9100-13 EM-CCD camera (SickKids Imaging Facility, Toronto, Canada). Serial optical sections were acquired at 0.3 µm and deconvolved using the Iterative Restoration function of Perkin Elmer Volocity 6.3 software (SickKids Imaging Facility, Toronto, Canada). A single focal plane (*xy* plane) was selected at a comparable depth in the tissue and an image was obtained using the Capture Snapshot function of Volocity. Images were then exported from Volocity and uniformly edited for brightness and contrast using Adobe Photoshop CS6.

Ommatidial mispatterning scores (OMS) were determined as previously described (Johnson and Cagan, 2009). An average OMS was calculated for each genotype and Student's *t*-test was used for statistical analysis and to determine *P*-values. Fluorescence intensity values across the 1°pc:IOC border were determined using the line tool in ImageJ. Puncta size and number were measured using the Volocity Measurements tool. Statistical analysis of puncta size, puncta number, average intensity and intensity ratios between WT and *Sac1^{ts}* was performed with Student's *t*-test using values normalized to WT. For fluorescence intensity and puncta measurements, non-neighboring IOCs or ommatidia in equivalent focal planes were selected for analysis. All experiments were replicated at least three times; quantification was performed using combined results from three independent experiments.

Acknowledgements

We thank J. Ashkenas, S. Egan, H. McNeill, R. Fehon and members of the Brill lab for helpful discussions; C.-I. J. Ma, J. Tan, L. Fabian and especially M. Pellikka for advice and assistance with experiments; L. Cooley, A. Kiger, U. Tepass, K.-F. Fischbach, J. Sisson and O. Papoulas, the Developmental Studies Hybridoma Bank, and the Bloomington *Drosophila* Stock Center for generously providing flies and reagents; M. Woodside and P. Paroutis (SickKids Imaging Facility) for assistance with confocal imaging and analysis; H. Hong and A. Darabie (Imaging Facility, Department of Cell & Systems Biology, University of Toronto) for assistance with TEM; D. Holmyard (Advanced Bioimaging Center, Mount Sinai Hospital) for assistance with SEM.

Competing interests

The authors declare no competing or financial interests.

Author contributions

Conceptualization: L.M.D.B., N.G., R.W., J.B., J.A.B.; Methodology: L.M.D.B., N.G., R.W., P.M., J.A.B.; Validation: L.M.D.B., N.G., A.B., P.M., J.A.B.; Formal analysis:

L.M.D.B., N.G., A.B.; Investigation: L.M.D.B., N.G., R.W., H.-C.W., A.B., J.B.; Resources: G.P., J.V.P., P.M., J.A.B.; Data curation: P.M., J.A.B.; Writing - original draft: L.M.D.B., J.A.B.; Writing - review & editing: L.M.D.B., N.G., R.W., H.-C.W., J.B., G.P., J.V.P., P.M., J.A.B.; Visualization: L.M.D.B., N.G., A.B., P.M., J.A.B.; Supervision: J.V.P., P.M., J.A.B.; Project administration: J.A.B.; Funding acquisition: J.V.P., P.M., J.A.B.

Funding

We gratefully acknowledge graduate scholarship funding from Natural Sciences and Engineering Research Council of Canada (NSERC) (to L.M.D.B. and J.B.), Ontario Graduate Scholarships (OGS) (to L.M.D.B., N.G. and J.B.), Canadian Institutes of Health Research (CIHR) (to L.M.D.B. and N.G.) and Hospital for Sick Children (SickKids) Restracomp (to L.M.D.B. and N.G.). This work was also funded by grants from NSERC (OGP 0105527-98 to J.V.P.; RGPIN-262166-10 to J.A.B.), British Columbia Health Research Foundation [#44 (97-2) and #151 (98-2) to J.V.P.], the National Institutes of Health (GM084088 to P.M.), the Cancer Research Society (#9059 and #11202 to J.A.B.); and CIHR (MOP-119483 to J.A.B.). Deposited in PMC for release after 12 months.

Supplementary information

Supplementary information available online at
http://dev.biologists.org/lookup/doi/10.1242/dev.151571.supplemental

References

Araujo, H., Machado, L. C. H., Octacílio-Silva, S., Mizutani, C. M., Silva, M. J. F. and Ramos, R. G. P. (2003). Requirement of the roughest gene for differentiation and time of death of interommatidial cells during pupal stages of Drosophila compound eye development. *Mech. Dev.* **120**, 537-547.

Ashburner, M. (1990). *Drosophila: A Laboratory Handbook*. Cold Spring Harbor, NY: Cold Spring Harbor Press.

Bao, S. and Cagan, R. (2005). Preferential adhesion mediated by Hibris and Roughest regulates morphogenesis and patterning in the Drosophila eye. *Dev. Cell* **8**, 925-935.

Bao, S., Fischbach, K.-F., Corbin, V. and Cagan, R. L. (2010). Preferential adhesion maintains separation of ommatidia in the Drosophila eye. *Dev. Biol.* **344**, 948-956.

Behnke, O. and Forer, A. (1967). Evidence for four classes of microtubules in individual cells. *J. Cell Sci.* **2**, 169-192.

Beronja, S., Laprise, P., Papoulas, O., Pellikka, M., Sisson, J. and Tepass, U. (2005). Essential function of Drosophila Sec6 in apical exocytosis of epithelial photoreceptor cells. *J. Cell Biol.* **169**, 635-646.

Blagoveshchenskaya, A., Cheong, F. Y., Rohde, H. M., Glover, G., Knödler, A., Nicolson, T., Boehmelt, G. and Mayinger, P. (2008). Integration of Golgi trafficking and growth factor signaling by the lipid phosphatase SAC1. *J. Cell Biol.* **180**, 803-812.

Brand, A. H. and Perrimon, N. (1993). Targeted gene expression as a means of altering cell fates and generating dominant phenotypes. *Development* **118**, 401-415.

Burgess, J., Del Bel, L. M., Ma, C.-I. J., Barylko, B., Polevoy, G., Rollins, J., Albanesi, J. P., Kramer, H. and Brill, J. A. (2012). Type II phosphatidylinositol 4-kinase regulates trafficking of secretory granule proteins in Drosophila. *Development* **139**, 3040-3050.

Cagan, R. L. and Ready, D. F. (1989a). The emergence of order in the Drosophila pupal retina. *Dev. Biol.* **136**, 346-362.

Cagan, R. L. and Ready, D. F. (1989b). Notch is required for successive cell decisions in the developing Drosophila retina. *Genes Dev.* **3**, 1099-1112.

Cheong, F. Y., Sharma, V., Blagoveshchenskaya, A., Oorschot, V. M., Brankatschk, B., Klumperman, J., Freeze, H. H. and Mayinger, P. (2010). Spatial regulation of Golgi phosphatidylinositol-4-phosphate is required for enzyme localization and glycosylation fidelity. *Traffic* **11**, 1180-1190.

Cleves, A. E., Novick, P. J. and Bankaitis, V. A. (1989). Mutations in the SAC1 gene suppress defects in yeast Golgi and yeast actin function. *J. Cell Biol.* **109**, 2939-2950.

Cordero, J. B., Larson, D. E., Craig, C. R., Hays, R. and Cagan, R. (2007). Dynamic decapentaplegic signaling regulates patterning and adhesion in the Drosophila pupal retina. *Development* **134**, 1861-1871.

Delage, E., Puyaubert, J., Zachowski, A. and Ruelland, E. (2013). Signal transduction pathways involving phosphatidylinositol 4-phosphate and phosphatidylinositol 4,5-bisphosphate: convergences and divergences among eukaryotic kingdoms. *Prog. Lipid Res.* **52**, 1-14.

De Matteis, M. A., Wilson, C. and D'Angelo, G. (2013). Phosphatidylinositol-4-phosphate: the Golgi and beyond. *BioEssays* **35**, 612-622.

Donoviel, D. B., Freed, D. D., Vogel, H., Potter, D. G., Hawkins, E., Barrish, J. P., Mathur, B. N., Turner, C. A., Geske, R., Montgomery, C. A. et al. (2001). Proteinuria and perinatal lethality in mice lacking NEPH1, a novel protein with homology to NEPHRIN. *Mol. Cell. Biol.* **21**, 4829-4836.

Dowler, S., Currie, R. A., Campbell, D. G., Deak, M., Kular, G., Downes, C. P. and Alessi, D. R. (2000). Identification of pleckstrin-homology-domain-containing proteins with novel phosphoinositide-binding specificities. *Biochem. J.* **351**, 19-31.

Faulhammer, F., Konrad, G., Brankatschk, B., Tahirovic, S., Knödler, A. and Mayinger, P. (2005). Cell growth-dependent coordination of lipid signaling and glycosylation is mediated by interactions between Sac1p and Dpm1p. *J. Cell Biol.* **168**, 185-191.

Fehon, R. G., Kooh, P. J., Rebay, I., Regan, C. L., Xu, T., Muskavitch, M. A. T. and Artavanis-Tsakonas, S. (1990). Molecular interactions between the protein products of the neurogenic loci Notch and Delta, two EGF-homologous genes in Drosophila. *Cell* **61**, 523-534.

Forrest, S., Chai, A., Sanhueza, M., Marescotti, M., Parry, K., Georgiev, A., Sahota, V., Mendez-Castro, R. and Pennetta, G. (2013). Increased levels of phosphoinositides cause neurodegeneration in a Drosophila model of amyotrophic lateral sclerosis. *Hum. Mol. Genet.* **22**, 2689-2704.

Foti, M., Audhya, A. and Emr, S. D. (2001). Sac1 lipid phosphatase and Stt4 phosphatidylinositol 4-kinase regulate a pool of phosphatidylinositol 4-phsophate that functions in the control of the actin cytoskeleton and vacuole morphology. *Mol. Biol. Cell* **12**, 2396-2411.

Gervais, L., Claret, S., Januschke, J., Roth, S. and Guichet, A. (2008). PIP5K-dependent production of PIP2 sustains microtubule organization to establish polarized transport in the Drosophila oocyte. *Development* **135**, 3829-3838.

Gillooly, D. J., Morrow, I. C., Lindsay, M., Gould, R., Bryant, N. J., Gaullier, J. M., Parton, R. G. and Stenmark, H. (2000). Localization of phosphatidylinositol 3-phosphate in yeast and mammalian cells. *EMBO J.* **19**, 4577-4588.

Godi, A., Di Campli, A., Konstantakopoulos, A., Di Tullio, G., Alessi, D. R., Kular, G. S., Daniele, T., Marra, P., Lucocq, J. M. and De Matteis, M. A. (2004). FAPPs control Golgi-to-cell-surface membrane traffic by binding to ARF and PtdIns(4)P. *Nat. Cell Biol.* **6**, 393-404.

Goldbach, P., Wong, R., Beise, N., Sarpal, R., Trimble, W. S. and Brill, J. A. (2010). Stabilization of the actomyosin ring enables spermatocyte cytokinesis in Drosophila. *Mol. Biol. Cell* **21**, 1482-1493.

Gorski, S. M., Brachmann, C. B., Tanenbaum, S. B. and Cagan, R. L. (2000). Delta and notch promote correct localization of irreC-rst. *Cell Death Differ.* **7**, 1011-1013.

Grzeschik, N. A. and Knust, E. (2005). IrreC/rst-mediated cell sorting during Drosophila pupal eye development depends on proper localisation of DE-cadherin. *Development* **132**, 2035-2045.

Guo, S., Stolz, L. E., Lemrow, S. M. and York, J. D. (1999). SAC1-like domains of yeast SAC1, INP52, and INP53 and of human synaptojanin encode polyphosphoinositide phosphatases. *J. Biol. Chem.* **274**, 12990-12995.

Hammond, G. R., Machner, M. P. and Balla, T. (2014). A novel probe for phosphatidylinositol 4-phosphate reveals multiple pools beyond the Golgi. *J. Cell Biol.* **205**, 113-126.

Hughes, W. E., Woscholski, R., Cooke, F. T., Patrick, R. S., Dove, S. K., McDonald, N. Q. and Parker, P. J. (2000). SAC1 encodes a regulated lipid phosphoinositide phosphatase, defects in which can be suppressed by the homologous Inp52p and Inp53p phosphatases. *J. Biol. Chem.* **275**, 801-808.

Inoue, Y. H., Savoian, M. S., Suzuki, T., Máthé, E., Yamamoto, M.-T. and Glover, D. M. (2004). Mutations in orbit/mast reveal that the central spindle is comprised of two microtubule populations, those that initiate cleavage and those that propagate furrow ingression. *J. Cell Biol.* **166**, 49-60.

Johnson, R. I. and Cagan, R. L. (2009). A quantitative method to analyze Drosophila pupal eye patterning. *PLoS ONE* **4**, e7008.

Kestilä, M., Lenkkeri, U., Männikkö, M., Lamerdin, J., McCready, P., Putaala, H., Ruotsalainen, V., Morita, T., Nissinen, M., Herva, R. et al. (1998). Positionally cloned gene for a novel glomerular protein–nephrin–is mutated in congenital nephrotic syndrome. *Mol. Cell* **1**, 575-582.

Ling, Y., Hayano, S. and Novick, P. (2014). Osh4p is needed to reduce the level of phosphatidylinositol-4-phosphate on secretory vesicles as they mature. *Mol. Biol. Cell* **25**, 3389-3400.

Liu, Y., Boukhelifa, M., Tribble, E. and Bankaitis, V. A. (2009). Functional studies of the mammalian Sac1 phosphoinositide phosphatase. *Adv. Enzyme Regul.* **49**, 75-86.

Manford, A. G., Stefan, C. J., Yuan, H. L., Macgurn, J. A. and Emr, S. D. (2012). ER-to-plasma membrane tethering proteins regulate cell signaling and ER morphology. *Dev. Cell* **23**, 1129-1140.

Marois, E., Mahmoud, A. and Eaton, S. (2006). The endocytic pathway and formation of the Wingless morphogen gradient. *Development* **133**, 307-317.

Mizuno-Yamasaki, E., Medkova, M., Coleman, J. and Novick, P. (2010). Phosphatidylinositol 4-phosphate controls both membrane recruitment and a regulatory switch of the Rab GEF Sec2p. *Dev. Cell* **18**, 828-840.

Nemoto, Y., Kearns, B. G., Wenk, M. R., Chen, H., Mori, K., Alb, J. G., Jr, De Camilli, P. and Bankaitis, V. A. (2000). Functional characterization of a mammalian Sac1 and mutants exhibiting substrate-specific defects in phosphoinositide phosphatase activity. *J. Biol. Chem.* **275**, 34293-34305.

Novick, P., Osmond, B. C. and Botstein, D. (1989). Suppressors of yeast actin mutations. *Genetics* **121**, 659-674.

Oda, H., Uemura, T., Harada, Y., Iwai, Y. and Takeichi, M. (1994). A Drosophila homolog of cadherin associated with armadillo and essential for embryonic cell-cell adhesion. *Dev. Biol.* **165**, 716-726.

Parnas, D., Haghighi, A. P., Fetter, R. D., Kim, S. W. and Goodman, C. S. (2001). Regulation of postsynaptic structure and protein localization by the Rho-type guanine nucleotide exchange factor dPix. *Neuron* **32**, 415-424.
Pellikka, M., Tanentzapf, G., Pinto, M., Smith, C., McGlade, C. J., Ready, D. F. and Tepass, U. (2002). Crumbs, the Drosophila homologue of human CRB1/RP12, is essential for photoreceptor morphogenesis. *Nature* **416**, 143-149.
Raucher, D., Stauffer, T., Chen, W., Shen, K., Guo, S., York, J. D., Sheetz, M. P. and Meyer, T. (2000). Phosphatidylinositol 4,5-bisphosphate functions as a second messenger that regulates cytoskeleton-plasma membrane adhesion. *Cell* **100**, 221-228.
Reiter, C., Schimansky, T., Nie, Z. and Fischbach, K. F. (1996). Reorganization of membrane contacts prior to apoptosis in the Drosophila retina: the role of the IrreC-rst protein. *Development* **122**, 1931-1940.
Riggleman, B., Schedl, P. and Wieschaus, E. (1990). Spatial expression of the Drosophila segment polarity gene armadillo is posttranscriptionally regulated by wingless. *Cell* **63**, 549-560.
Rivas, M. P., Kearns, B. G., Xie, Z., Guo, S., Sekar, M. C., Hosaka, K., Kagiwada, S., York, J. D. and Bankaitis, V. A. (1999). Pleiotropic alterations in lipid metabolism in yeast sac1 mutants: relationship to "bypass Sec14p" and inositol auxotrophy. *Mol. Biol. Cell* **10**, 2235-2250.
Rohde, H. M., Cheong, F. Y., Konrad, G., Paiha, K., Mayinger, P. and Boehmelt, G. (2003). The human phosphatidylinositol phosphatase SAC1 interacts with the coatomer I complex. *J. Biol. Chem.* **278**, 52689-52699.
Roth, L. E. (1967). Electron microscopy of mitosis in amebae. 3. Cold and urea treatments: a basis for tests of direct effects of mitotic inhibitors on microtubule formation. *J. Cell Biol.* **34**, 47-59.
Roy, A. and Levine, T. P. (2004). Multiple pools of phosphatidylinositol 4-phosphate detected using the pleckstrin homology domain of Osh2p. *J. Biol. Chem.* **279**, 44683-44689.
Ruotsalainen, V., Ljungberg, P., Wartiovaara, J., Lenkkeri, U., Kestila, M., Jalanko, H., Holmberg, C. and Tryggvason, K. (1999). Nephrin is specifically located at the slit diaphragm of glomerular podocytes. *Proc. Natl. Acad. Sci. USA* **96**, 7962-7967.
Santiago-Tirado, F. H. and Bretscher, A. (2011). Membrane-trafficking sorting hubs: cooperation between PI4P and small GTPases at the trans-Golgi network. *Trends Cell Biol.* **21**, 515-525.
Satoh, D., Hirose, T., Harita, Y., Daimon, C., Harada, T., Kurihara, H., Yamashita, A. and Ohno, S. (2014). aPKClambda maintains the integrity of the glomerular slit diaphragm through trafficking of nephrin to the cell surface. *J. Biochem.* **156**, 115-128.
Schneider, T., Reiter, C., Eule, E., Bader, B., Lichte, B., Nie, Z., Schimansky, T., Ramos, R. G. P. and Fischbach, K.-F. (1995). Restricted expression of the irreC-rst protein is required for normal axonal projections of columnar visual neurons. *Neuron* **15**, 259-271.
Sisson, J. C., Field, C., Ventura, R., Royou, A. and Sullivan, W. (2000). Lava lamp, a novel peripheral golgi protein, is required for Drosophila melanogaster cellularization. *J. Cell Biol.* **151**, 905-918.
Stauffer, T. P., Ahn, S. and Meyer, T. (1998). Receptor-induced transient reduction in plasma membrane PtdIns(4,5)P2 concentration monitored in living cells. *Curr. Biol.* **8**, 343-346.
Tahirovic, S., Schorr, M. and Mayinger, P. (2005). Regulation of intracellular phosphatidylinositol-4-phosphate by the Sac1 lipid phosphatase. *Traffic* **6**, 116-130.
Tan, J. and Brill, J. A. (2014). Cinderella story: PI4P goes from precursor to key signaling molecule. *Crit. Rev. Biochem. Mol. Biol.* **49**, 33-58.
Tan, J., Oh, K., Burgess, J., Hipfner, D. R. and Brill, J. A. (2014). PI4KIIIα is required for cortical integrity and cell polarity during Drosophila oogenesis. *J. Cell Sci.* **127**, 954-966.
Tilney, L. G. and Porter, K. R. (1967). Studies on the microtubules in heliozoa. II. The effect of low temperature on these structures in the formation and maintenance of the axopodia. *J. Cell Biol.* **34**, 327-343.
Vega, I. E. and Hsu, S.-C. (2001). The exocyst complex associates with microtubules to mediate vesicle targeting and neurite outgrowth. *J. Neurosci.* **21**, 3839-3848.
Velichkova, M., Juan, J., Kadandale, P., Jean, S., Ribeiro, I., Raman, V., Stefan, C. and Kiger, A. A. (2010). Drosophila Mtm and class II PI3K coregulate a PI(3)P pool with cortical and endolysosomal functions. *J. Cell Biol.* **190**, 407-425.
von Stein, W., Ramrath, A., Grimm, A., Muller-Borg, M. and Wodarz, A. (2005). Direct association of Bazooka/PAR-3 with the lipid phosphatase PTEN reveals a link between the PAR/aPKC complex and phosphoinositide signaling. *Development* **132**, 1675-1686.
Walther, R. F. and Pichaud, F. (2006). Immunofluorescent staining and imaging of the pupal and adult Drosophila visual system. *Nat. Protoc.* **1**, 2635-2642.
Wei, H.-C., Rollins, J., Fabian, L., Hayes, M., Polevoy, G., Bazinet, C. and Brill, J. A. (2008). Depletion of plasma membrane PtdIns(4,5)P2 reveals essential roles for phosphoinositides in flagellar biogenesis. *J. Cell Sci.* **121**, 1076-1084.
Wei, H.-C., Sanny, J., Shu, H., Baillie, D. L., Brill, J. A., Price, J. V. and Harden, N. (2003a). The Sac1 lipid phosphatase regulates cell shape change and the JNK cascade during dorsal closure in *Drosophila*. *Curr. Biol.* **13**, 1882-1887.
Wei, H.-C., Shu, H. and Price, J. V. (2003b). Functional genomic analysis of the 61D-61F region of the third chromosome of Drosophila melanogaster. *Genome* **46**, 1049-1058.
Whitters, E. A., Cleves, A. E., McGee, T. P., Skinner, H. B. and Bankaitis, V. A. (1993). SAC1p is an integral membrane protein that influences the cellular requirement for phospholipid transfer protein function and inositol in yeast. *J. Cell Biol.* **122**, 79-94.
Wolff, T. and Ready, D. F. (1991). Cell death in normal and rough eye mutants of Drosophila. *Development* **113**, 825-839.
Yavari, A., Nagaraj, R., Owusu-Ansah, E., Folick, A., Ngo, K., Hillman, T., Call, G., Rohatgi, R., Scott, M. P. and Banerjee, U. (2010). Role of lipid metabolism in smoothened derepression in hedgehog signaling. *Dev. Cell* **19**, 54-65.